



# A Second-Order Maximum-Entropy-Inspired Interpolative Moment Closure Technique for the Prediction of Radiative Heat Transfer in Non-Gray Participating Media

Joachim A. R. Sarr\* and Clinton P. T. Groth†

*University of Toronto Institute for Aerospace Studies  
4925 Dufferin Street, Toronto, Ontario, M3H 5T6, Canada*

An efficient and hyperbolic interpolative-based second-order maximum entropy,  $M_2$ , moment closure for providing approximate numerical solutions to the equation of radiative transfer in non-gray participating media is proposed and described. This newly-developed non-gray moment closure technique results in significant computational savings compared to an approach that makes use of the direct numerical solution of the optimization problem for entropy maximization. Theoretical details of the proposed interpolative-based second-order moment closure, along with a description of an efficient Godunov-type finite-volume scheme that has been developed for the numerical solution of the resulting system of hyperbolic moment equations, are presented. The finite-volume method makes use of limited linear solution reconstruction, multi-block body-fitted quadrilateral meshes with anisotropic adaptive mesh refinement (AMR), and an efficient Newton-Krylov-Schwarz (NKS) iterative method for solution of the resulting non-linear algebraic equations arising from the spatial discretization procedure. The predictive capabilities of the proposed interpolative non-gray  $M_2$  closure are assessed by comparing its solutions to those of its lower-order counterpart, i.e., the non-gray first-order,  $M_1$ , maximum entropy moment closure. The comparisons also include the more commonly adopted first-order,  $P_1$ , and third-order,  $P_3$ , spherical harmonic moment closures, as well as the popular discrete ordinates method (DOM). The latter is used as a benchmark for the comparisons whenever exact analytical solutions of the radiative transfer equation (RTE) are not available. The assessment is performed for a number of representative problems involving non-gray radiative heat transfer between parallel plates as well as within rectangular enclosures. The strong spectral dependence exhibited by the absorption coefficient of radiatively participating real gases is treated using a statistical narrow-band correlated- $k$  model. The numerical results for all the problems studied show that the non-gray  $M_2$  maximum-entropy moment closure provides improved predictions of the radiation solutions compared to the non-gray  $M_1$  and  $P_1$  closures, and is, in most cases, superior to the  $P_3$  spherical harmonic moment closure, while achieving similar levels of accuracy compared to the standard discrete ordinates method.

## Nomenclature

|          |   |
|----------|---|
| $c$      | speed of light in vacuum                  |
| $h$      | Planck constant                           |
| $k$      | Boltzmann constant                        |
| $n$      | occupation number                         |
| $C_1$    | first radiation constant                  |
| $I_\eta$ | spectral radiative intensity distribution |

\*PhD Candidate, Email: joachimandre.sarr@mail.utoronto.ca

†Professor, Email: groth@utias.utoronto.ca, AIAA Associate Fellow.

|                |  |
|----------------|--|
| $I_g$          | reordered radiative intensity distribution           |
| $I_{b\eta}$    | spectral blackbody intensity                         |
| $\kappa_\eta$  | spectral absorption coefficient ( $\text{m}^{-1}$ )  |
| $k(g)$         | reordered absorption coefficient ( $\text{m}^{-1}$ ) |
| $\sigma_\eta$  | spectral scattering coefficient                      |
| $\Phi_\eta$    | spectral scattering phase function                   |
| $I_\eta^{(n)}$ | spectral angular moment or order $n$                 |
| $I_g^{(n)}$    | reordered angular moment or order $n$                |
| $N^{(n)}$      | normalized angular moment or order $n$               |
| $\vec{s}$      | direction of propagation of radiation                |
| $h_R$          | radiative entropy                                    |
| $M_N$          | maximum entropy moment closure of order $N$          |
| $P_N$          | spherical harmonic moment closure of order $N$       |

*Subscript*

|        |                      |
|--------|----------------------|
| $\eta$ | wavenumber           |
| $g$    | reordered wavenumber |

## I. Introduction

The equation governing the transport of radiative energy within a participating media, which is commonly referred to as the radiative transfer equation (RTE), is a complex nonlinear integro-differential equation with high dimensionality, since the distribution of radiation is a function of seven independent variables. The high dimensionality, combined with high nonlinearity, makes it impossible to derive general exact analytical solutions for the RTE in the general case, and approximate solutions of the latter equation are generally obtained by numerical means.

In addition to its spatial and temporal dependencies, the radiative intensity distribution is also a function of frequency or wavenumber and direction of propagation of radiation. While the spatial and temporal variations are commonly treated using traditional finite-volume schemes for the solution of discrete governing equations over finite control volumes,<sup>1-6</sup> and the spectral dependence can be tackled by means of state-of-the-art spectral radiation techniques,<sup>7-10</sup> the treatment of the directional dependence of the radiative intensity distribution, for accurate and efficient predictions of macroscopic radiative quantities, is still an active research subject. The discrete ordinates method (DOM)<sup>11</sup> is one of the most widely used techniques for approximating the angular dependence of the RTE. Solutions of the DOM are generally obtained using space marching iterative techniques, which are known to be very efficient for problems with relatively simple geometry and simplified physics (e.g., non-scattering media). However, space marching techniques can lose their effectiveness in cases with complex three-dimensional geometries and realistic physics, as is the case in many practical applications. The method of moments<sup>12</sup> provides a hierarchy of models allowing a possible reduction in the numerical costs associated with solving the RTE by replacing the representation of the angular dependence of the radiative distribution by a finite set of angular integrals or moments of the latter. However, closure is required for the finite system of equations for the angular moments since there are always more unknowns than equations. The spherical harmonic moment closures ( $P_N$ , where  $N$  refers to the order of the highest moments in the closed system), has been extensively used for providing approximate radiation heat transfer solutions,<sup>13-16</sup> where the underlying radiative intensity distribution is approximated by a truncated series expansion in terms of orthogonal spherical harmonic functions. Closed-form analytic expressions for the closing relations of the  $P_N$  closures exist for any order of approximation,  $N$ . However, one of the main limitations of the  $P_N$  moment closures is their inability to properly capture highly anisotropic regimes. In fact, in such regimes, the distribution of radiation is uniquely determined by a Dirac-delta, which is almost impossible to reproduce with a polynomial expansion of the radiative intensity distribution, as in the  $P_N$  closures.

As alternatives to the spherical harmonic approximation of the radiative intensity distribution, there has recently been particular interest in maximum-entropy-based,  $M_N$ , moment closures to the system of moment equations arising from the RTE.<sup>17</sup> Approaches based on the principle of maximization of entropy are particularly attractive for several reasons, among which is the fact that, for a given finite set of moments,

they provide the most likely form of the radiative intensity distribution among all the possible forms that can reproduce such set of moments.<sup>18</sup> Moreover, the resulting closed system of moment equations is strictly hyperbolic and the moments associated with the reconstructed entropy-maximizing distribution of radiation are physically realizable. Furthermore, even the lowest-order maximum-entropy moment closure, namely the first-order,  $M_1$ , closure, can capture highly anisotropic distributions of radiative intensity. However, unlike the  $P_N$  moment closures, closed-form analytic expressions for the closing relations of the  $M_N$  closures only exist for the gray  $M_1$  closure in the case of Bose-Einstein entropy for radiation. Repeated numerical solution of the optimization problem for entropy maximization is therefore generally required, whenever an update of the radiation solutions is required, which can make the application of the  $M_N$  closures computationally prohibitive. In spite of these difficulties, in a previous study, Hauck<sup>19,20</sup> explored the predictive capabilities of maximum entropy moment closures up to sixth-order, based on the Boltzmann entropy of radiation, for various test problems involving gray-gas radiative heat transfer in one-dimensional slab geometries. In this study, the solutions of the aforementioned  $M_N$  closures were obtained by solving the optimization problem for entropy maximization via a numerical approach. Furthermore, Hauck compared the predictions of the aforementioned  $M_N$  closures to those of the  $P_N$  spherical harmonic approximations. His analysis clearly demonstrated that the higher-order  $M_N$  closures provided significantly improved predictions of radiative heat transfer, relative to the  $M_1$  closure, which produces a nonphysical behaviour in the radiative energy density in situations where there is more than one primary direction for the propagation of the radiative energy.<sup>21</sup> Similar results have been obtained by Monreal and Frank,<sup>22</sup> who proposed an analytical approximation for the  $M_2$  closing relation in the one-dimensional case.

Motivated by a desire for moment closures for radiative transport applications which have the desirable properties of the  $M_N$  closures without the prohibitive computational costs associated with repeated solution of the optimization problem for entropy maximization, Pichard *et al.*<sup>23</sup> recently proposed interpolative-based approximations of the closure relations for both the gray  $M_1$  and  $M_2$  moment closures, obeying Boltzmann statistics, in multiple space dimensions. In the context of the  $M_1$  closure, Pichard *et al.*<sup>23</sup> developed an interpolative-based analytical approximation of the Eddington factor. The proposed interpolation is based on a convex combination of the known analytical expressions of the Eddington factor on the upper and lower boundaries of the space of realizable angular moments up to second-order. The convex interpolant is then determined such that the values of the Eddington factor as well as its first derivatives, both on the boundaries of the realizable space up to first-order and in the isotropic limit, are exactly reproduced. In addition, the interpolant was also chosen such that the error between the proposed approximation and pre-computed solutions of the optimization problem for entropy maximization, for sets of angular moments uniformly spanning the full realizable space up to first-order, is minimized. For the interpolative-based approximation of the gray  $M_2$  closure in multiple space dimensions, Pichard *et al.*<sup>23</sup> first performed interpolations in the 1D case, based on convex combinations of the known exact form of the closure relations on the upper and lower boundaries of the realizability domain for angular moments up to third order. However, since, to date, necessary and sufficient conditions for realizability of the third-order angular moments in multiple space dimensions do not exist, the extension of the interpolation to multidimensional physical space was then carried out in the realizable domain for moments up to first order, the latter being a subset of the full realizable space for the  $M_2$  closure, which involves moments up to second order.

By way of its construction, the resulting interpolation procedure proposed by Pichard *et al.*<sup>23</sup> only mimics accurately the corresponding maximum entropy solutions in one dimensional physical space, but not in multiple space dimensions. Moreover, the fact that the construction in multiple dimensions is based on the realizability domain for moments up to just first order does not take into account the possible regimes that can only be described by higher-order moments describing the realizable space for the  $M_2$  closure. More recently Sarr and Groth<sup>24,25</sup> proposed a new interpolative-based approximation of the gray  $M_2$  closure, in the case of Bose-Einstein-based entropy of radiation. Unlike Pichard *et al.*,<sup>23</sup> the  $M_2$  closure of Sarr and Groth<sup>24,25</sup> mimics fully the maximum entropy solutions everywhere within the realizable space for angular moments up to second-order in multiple space dimensions. It should also be pointed out that an extended quadrature method of moments (EQMOM)-based second-order moment closure was developed by Li *et al.*,<sup>26</sup> as an approximation to the  $M_2$  maximum-entropy closure. In their approach, the base function used in the EQMOM scheme are  $\beta$  probability density functions. One of the main advantages of this so-called  $B_2$  model of Li *et al.*,<sup>26</sup> compared to the  $M_2$  closure, is the existence of closed-form analytical expressions for the closure relations. Moreover, the  $B_2$  model provides a smooth interpolation between the isotropic and the free-streaming limits. However, the EQMOM-based closure does not really attempt to mimic closely the

properties of the  $M_2$  maximum entropy closure and the  $B_2$  model in multiple space dimensions is neither globally realizable nor globally hyperbolic. In fact, Li *et al.*<sup>26</sup> have shown that the quadrature-based approximation to the  $M_2$  closure is only realizable and hyperbolic in a portion of the realizable space defined by moments up to second-order.

To the authors' knowledge, the only previous study concerned with investigating the predictive capabilities of the non-gray maximum-entropy moment closures for the non-gray case is due to Turpault.<sup>27,28</sup> More specifically, the latter formulated a multigroup variant of the non-gray  $M_1$  closure, whereby the spectrally dependent form of the entropy maximizing distribution was approximated by averages over groups of frequencies, spanning the spectrum of interest for the computations. For any given set of band-averaged angular moments up to first-order, the Eddington factor, which is the only unknown parameter in the closing relations, was then obtained by numerically solving the underlying dual optimization problem for entropy maximization for the corresponding frequency group. As mentioned previously, the repeated solution of the optimization problem for entropy maximization is expensive, and should be avoided, especially when radiation must be coupled with other phenomena, as is the case in large-scale simulations for practical engineering problems. Moreover, the multigroup approach, which consists of approximating spectral radiative quantities over a given group of frequencies by an average over that set, may lead to substantial over- or under-estimations of the spectrally integrated radiative quantities, due to the strong spectral dependence of the absorption coefficient of real gases.<sup>29</sup> Such strong variations of the absorption coefficient with respect to frequency have led to the development of efficient, state-of-the-art spectral techniques for efficient integration of radiative quantities over the full spectrum of frequencies, including the Statistical Narrow-Band Correlated- $k$  (SNBCK)<sup>7</sup> model, which is of interest in this study. The SNBCK technique is based on re-ordering of the strongly varying spectral absorption coefficient into a monotonic function of a cumulative distribution function, and can yield comparable accuracy with respect to the straightforward and very expensive line-by-line calculations,<sup>29</sup> but with substantial improvements in computational efficiency relative to the latter. In light of these observations, it seems crucial to develop efficient interpolative-based non-gray maximum-entropy moment closures that accurately mimic numerical solutions of the maximum entropy optimization problem and also couple naturally with the SNBCK, so as to take full advantage of the computational benefits provided by the latter spectral techniques, for radiation calculations in real gases.

In a recent paper by the authors,<sup>30</sup> an interpolative-based approximation of the Eddington factor for the second-order closing fluxes of the non-gray  $M_1$  closure has been proposed and described, followed by an assessment of its predictive capabilities in laminar reactive flows with soot formation. Improvements to the latter non-gray  $M_1$  closure have been proposed in a more recent paper by Sarr and Groth,<sup>31</sup> which results in a more robust, realizable and hyperbolic closed system of moment equations up to first-order. In particular, the more recent study of Sarr and Groth<sup>31</sup> follows a more systematic approach for the choice of the mapping of the radiative energy density, for the purpose of the interpolation procedure. More specifically, instead of an algebraic mapping, with arbitrarily fixed value for the mapping length scale,<sup>30</sup> an exponential mapping of the energy density was adopted in,<sup>31</sup> the length scale of which was chosen to be a free parameter. The distribution of such a length scale was then chosen such that the proposed interpolative-based approximation of the Eddington factor is realizable and accurately mimics numerical solutions of the optimization problem for entropy maximization over the full realizable space for angular moments up to first order and over the full spectrum of frequencies, while yielding a hyperbolic closed system of moment equations.

The aim of this study is to develop a new, efficient and hyperbolic interpolative-based analytical approximation of the closing relations for the non-gray  $M_2$  closure, in the case of the entropy of radiation based on Bose-Einstein statistics. Our proposed interpolation procedure mimics very closely the solution quality and desirable properties of the original non-gray  $M_2$  closure, while avoiding the relatively computationally expensive iterative numerical solution procedure, associated with the entropy maximization problem, in practical simulations. The proposed construction is very similar to the one adopted by Sarr and Groth<sup>24,25</sup> for the interpolative-based  $M_2$  closure for gray radiation, with some improvements in the polynomial interpolation procedure, yielding an overall more computationally efficient approximation of the maximum-entropy-based third-order closing fluxes. More specifically, unlike the  $M_2$  closure proposed by Pichard *et al.*,<sup>23</sup> the third-order closing fluxes of the non-gray  $M_2$  closure are approximated by a smooth interpolant of their known exact analytical expressions at some of the boundaries of the realizable space for the second-order angular moments. Moreover, for each of the closing fluxes being approximated, the interpolant is defined as an expansion of orthogonal polynomials, the coefficients of which are determined via solution of the Vandermonde system associated with suitably chosen interpolation nodes, so as to provide quasi-optimal approximations

of the quantities of interest. By means of its construction, our proposed interpolative-based procedure accurately reproduces derivatives of the closing fluxes on some of the boundaries of the realizable space for angular moments up to second-order, and also accurately approximates numerical maximum entropy solutions associated with sets of angular moments spanning the full realizable space of interest. Furthermore, unlike Pichard *et al.*<sup>23</sup> and Sarr and Groth,<sup>24,25</sup> where the assumption of a gray media was invoked, our proposed interpolation procedure also involves a particular treatment of the spectral dependence of the third-order closing fluxes. More specifically, in this study, the procedure described in the previous work of Sarr and Groth,<sup>31</sup> for the accurate treatment of the spectral dependence of the Eddington factor in the case of the non-gray  $M_1$  closure, is adopted and extended to the case of the non-gray  $M_2$  closure, which results in a robust and accurate approximation of maximum entropy solutions for the third-order closing fluxes over the full realizable space for angular moments up to second-order, as well as over the full spectrum of frequencies.

After presenting the theoretical details of the interpolation procedure for our new non-gray  $M_2$  closure, its particular implementation in the context of the state-of-the-art statistical narrow-band correlated- $k$  (SNBCK) model,<sup>7</sup> is discussed. Next, an efficient Godunov-type finite-volume scheme is described for the numerical solution of the resulting system of hyperbolic moment equations arising from our non-gray  $M_2$  interpolative-based closure. Finally, the predictive capabilities of the newly developed non-gray  $M_2$  closure are assessed by comparing its solutions to those of its first-order counterpart.<sup>31</sup> The comparisons are also concerned with the solutions of the more commonly adopted  $P_1$  and  $P_3$  spherical harmonic moment closures, as well as the popular and standard DOM. The assessments, which, for now, are only concerned with solution accuracy, are performed by means of several representative test problems involving non-gray radiative heat transfer between parallel plates and within rectangular enclosures, whereby the medium composition and temperature distribution are predetermined. The solutions of the DOM are used here as a reference for the comparisons, whenever exact analytical solutions of the RTE are not available.

## II. Radiation Transport in Non-Gray Participating Media

The transport of radiant energy in physical space,  $\vec{x}$ , and time,  $t$ , in the direction of propagation,  $\vec{s}$ , at a given wavenumber,  $\eta$ , in a radiatively participating media with absorption coefficient,  $\kappa_\eta = \kappa_\eta(\vec{x}, t)$  and scattering coefficient,  $\sigma_{s\eta} = \sigma_{s\eta}(\vec{x}, t)$ , is described by the radiative transfer equation, which has the form<sup>32</sup>

$$\frac{1}{c} \frac{\partial I_\eta}{\partial t} + \vec{s} \cdot \vec{\nabla} I_\eta = \kappa_\eta I_{b\eta} - (\kappa_\eta + \sigma_{s\eta}) I_\eta + \frac{\sigma_{s\eta}}{4\pi} \int_{4\pi} I_\eta(\vec{s}') \Phi_\eta(\vec{s}', \vec{s}) d\Omega', \quad (1)$$

where  $c$  is the speed of light in a vacuum,  $I_\eta = I_\eta(\vec{x}, \vec{s}, t)$  is the spectral radiative intensity,  $I_{b\eta} = I_{b\eta}(T)$  (where  $T = T(\vec{x}, t)$  is the temperature field) is the spectral Planck function or blackbody intensity,  $\Omega$  denotes solid angle, and  $\Phi_\eta(\vec{s}', \vec{s})$  is the scattering phase function. The latter can be thought of as describing the probability that a ray travelling in direction,  $\vec{s}'$ , will be scattered into direction,  $\vec{s}$ , and is also a function of location in space and time. The subscript,  $\eta$ , indicates a spectrally varying or dependent quantity.

The RTE, as given in Eq. (1), is a complex nonlinear equation with high dimensionality (7 independent variables) for which there exists no general exact analytical solution. As such, one must therefore rely on techniques based on approximate treatments on the independent variables. The temporal and spatial dependencies can be treated using standard finite-volume techniques for hyperbolic equations. The rather strong spectral dependence of the radiative properties of real gases, more specifically the spectral absorption coefficient,  $\kappa_\eta$ , will be treated herein using the statistical narrow-band correlated- $k$  (SNBCK) model.<sup>7</sup> For the angular dependence of the spectral radiative intensity distribution, different approximate treatments will be considered, including the discrete ordinates method, the spherical harmonics,  $P_N$ , and the maximum entropy,  $M_N$ , moment closures, the latter being the focus of the present study.

### II.A. Discrete Ordinates Method (DOM)

In the DOM,<sup>11</sup> angular quadrature is used to transform the equation of radiative transfer into a set of partial-differential equations (PDEs) with only spatial and temporal dependence. The angular discretization technique makes use of the assumption that the radiation is transported only along a finite set of discrete directions, instead of the effectively infinite number of directions allowed in Eq. (1) by a continuous representation of the solid angle. In other words, the solid angle is divided into a finite number,  $M$ , of discrete directions (or ordinates)  $\vec{s}_m$ ,  $m = 1, \dots, M$ . In this way, the RTE is transformed into a system of  $M$  coupled

equations given by

$$\frac{1}{c} \frac{\partial I_{\eta,m}}{\partial t} + \vec{s}_m \cdot \vec{\nabla} I_{\eta,m} = \kappa_{\eta} I_{b\eta} - (\kappa_{\eta} + \sigma_{s\eta}) I_{\eta,m} + \frac{\sigma_{s\eta}}{4\pi} \sum_{n=1}^M w_n I_{\eta,n} \Phi_{\eta}(\vec{s}_n, \vec{s}_m), \quad (2)$$

where the subscript  $m$  denotes the discrete ordinate direction,  $I_{\eta,m}$  is the radiative intensity in the  $m^{\text{th}}$  direction and  $w_m$  is the quadrature weight associated with the direction  $\vec{s}_m$ . Several quadrature rules have been developed for the DOM, including the  $S_N$  schemes of Lathrop and Carlson<sup>33</sup> and the  $T_N$  schemes of Thurgood *et al.*<sup>34</sup> The  $T_4$  quadrature scheme is used in this study for all of the reported DOM simulation results.

The DOM has been used extensively to provide approximate solutions to the RTE due to its good balance between accuracy and computational efficiency. However, this direct discretization technique is associated with two major limitations:<sup>35</sup> false scattering and ray effects. The former is due to the spatial discretization of the RTE whereas the latter is related to the discretization of the angular distribution of the radiative intensity. Several approaches have been proposed in order to cope with such issues.<sup>34,36–40</sup> Additionally, as mentioned in the introduction, the space marching techniques commonly used to solve the resulting discretized equations of the DOM can be extremely efficient for relatively simple geometries and physics; however, the space marching techniques may exhibit poor convergence for applications involving complex three-dimensional geometries and complex physics<sup>5</sup> (e.g., highly scattering media, turbulent reactive flows, etc.).

### III. Moment Closure Methods for Solution of the RTE

An alternative approach to the treatment of the angular dependence of the radiative intensity distribution, as carried out in the DOM, involves solving directly for the angular integrals or macroscopic moments of the distribution. These angular moments,  $I_{\eta}^{(n)}$ , are taken with respect to angular weights  $\vec{s}^n = \vec{s} \otimes \dots \otimes \vec{s}$ , for  $n = 0, \dots, \infty$ , whose independent entries form a monomial basis, and have the form

$$\begin{aligned} I_{\eta}^{(n)}(\vec{x}, t) &= \langle \vec{s}^n I_{\eta}(\vec{x}, \vec{s}, t) \rangle \\ &= \int_{4\pi} \vec{s}^n I_{\eta}(\vec{x}, \vec{s}, t) d\Omega = \int_0^{2\pi} \int_0^{\pi} \vec{s}^n I_{\eta}(\vec{x}, \vec{s}, t) \sin \theta d\theta d\psi. \end{aligned} \quad (3)$$

The first few angular moments, as defined in Eq. (3), are related to some well-known physical quantities. More specifically, the zeroth-order moment,  $I_{\eta}^{(0)}$ , which is a scalar, is related to the radiative energy density, the first-order moment,  $I_{\eta}^{(1)}$ , a 3-component vector in three-dimensional space, is associated with the radiative flux, and finally, the second-order moment,  $I_{\eta}^{(2)}$ , which is a second-order tensor with 6 independent entries in three dimensions, is associated to the radiative pressure. Beyond second-order, the angular moments, which then correspond to symmetric tensors of order at least three, have no well-established physical interpretation. We also define the normalized angular moments of order  $n$ , denoted by  $N^{(n)}$ , as follows

$$N^{(n)} = \frac{I_{\eta}^{(n)}}{I_{\eta}^{(0)}}. \quad (4)$$

Taking angular integrals of the RTE, Eq. (1), results in a system of moment equations of infinite size characterizing uniquely an arbitrary distribution. Solving such an infinite system of equations is however obviously unfeasible from a practical viewpoint. Instead, a reduced finite set of moments and their transport equations are considered, in practice. In this case however, a solution to the so-called closure problem is then required as the resulting system of transport equations for the finite set of moments generally involves the next higher-order moments. In particular, additional expressions relating the highest-order moments to the known lower-order moments are required for closure. These so-called closing relations are usually obtained via the reconstruction of an assumed form for the underlying non-negative angular distribution in terms of the known finite set of lower-order moments. There exists a wide range of possible forms for such an approximate distribution. In fact, there is effectively an infinite set of possible distributions sharing the same set of known lower-order moments. However, the choice of the approximate form generally dictates the many important mathematical properties of the resulting closed system of moment equations: namely the

realizability of the predicted moments and hyperbolicity of the moment equations. A set of moments is said to be physically realizable if there exists a strictly non-negative-valued distribution of the radiative intensity that will yield the given moments.<sup>3</sup> The set of all realizable moments up to a given order  $n$  then defines the so-called  $n$ -dimensional phase space of physically realizable moments and is denoted here as  $\mathcal{R}^{(n)}$ . This region is generally described by a set of inequalities on the values of the moments: the so-called moment realizability conditions. In this study, approximate forms for the angular distribution resulting from the spherical harmonic approximation as well as the principle of maximization of entropy will be considered and their application to radiative transport in non-gray media will be the primary focus.

Another important consideration for the moment closure techniques outlined above is the selection or choice of the number of moments to be included in the closure of interest, and which are subsequently used to reconstruct the approximate angular intensity distribution. In general, only the zeroth- and first-order moments, namely the radiative energy density,  $I_\eta^{(0)}$ , and the radiative heat flux,  $I_\eta^{(1)}$ , respectively, are of primary interest in engineering applications. However, the more angular moments that are used in the closure to reconstruct the approximate distribution, the wider the range of optical conditions that may be captured accurately by the closure.

### III.A. $P_N$ Spherical Harmonic Moment Closures

In the spherical harmonic moment closures, the spectrally dependent radiative intensity distribution,  $I_\eta(\vec{x}, \vec{s}, t)$ , is expressed as a series expansion in terms of the orthogonal spherical harmonic functions as follows<sup>41, 42</sup>

$$I_\eta(\vec{x}, \vec{s}, t) = \sum_{n=0}^N \sum_{m=-n}^n I_{n,\eta}^m(\vec{x}, t) Y_n^m(\vec{s}), \quad (5)$$

where  $N$  is the order of the highest moment in the closed system,  $I_{n,\eta}^m(\vec{x}, t)$  are location-dependent coefficients of the series expansion which can be directly related to the known finite set of moments, and  $Y_n^m(\vec{s})$  is the spherical harmonic function of degree  $n$  and order  $m$  having the form

$$Y_n^m(\vec{s}) = \begin{cases} \cos(m\psi) P_n^m(\cos\theta), & \text{for } m \geq 0, \\ \sin(|m|\psi) P_n^{|m|}(\cos\theta), & \text{for } m < 0, \end{cases} \quad (6)$$

and where  $P_n^m(\cos\theta)$  is the associated Legendre polynomial.

### III.B. First-Order $P_1$ Spherical Harmonic Moment Closure

The first-order  $P_1$  spherical harmonic approximation provides closure to the system of transport equations for angular moments up to first-order, which only involves transport equations for the zeroth- and first-order moments,  $I_\eta^{(0)}$  and  $I_\eta^{(1)}$ , respectively (i.e., a set of four moments in three space dimensions for the radiative energy density and fluxes in each coordinate direction). This is achieved by approximating the distribution using the form given in Eq. (5), with  $N = 1$ , which is then reconstructed in terms of angular moments up to first order. The second-order moment,  $I_\eta^{(2)}$ , is a dyadic quantity (i.e., a second-order tensor) and is involved in the transport equation for  $I_\eta^{(1)}$ . This quantity can be directly expressed in terms of the lower-order moments via integration of the reconstructed distribution, yielding

$$I_{ij,\eta}^{(2)} = \frac{\delta_{ij}}{3} I_\eta^{(0)}, \quad (7)$$

where  $\delta_{ij}$  is the Kronecker delta operator. This is the so-called  $P_1$  approximation, which is generally considered to be accurate only for optically thick media as it is associated with nearly-isotropic distributions of the radiative intensity.

### III.C. Third-Order $P_3$ Spherical Harmonic Moment Closure

For comparisons to the proposed non-gray  $M_1$  interpolative closure, the third-order spherical harmonic,  $P_3$ , moment closure is also considered here. The  $P_3$  approximation provides closure to the system of transport equations for angular moments up to third-order (i.e.,  $I_\eta^{(0)}$ ,  $I_\eta^{(1)}$ ,  $I_\eta^{(2)}$ , and  $I_\eta^{(3)}$ ), where the transport equations

for the third-order moments involve the fourth-order moments,  $I_\eta^{(4)}$ . More specifically, the fourth-order moments are expressed in terms of the lower order moments by making use of the form for the distribution, given in Eq. (5), with known angular moments up to third-order, and the resulting closing relations can be summarized as follows

$$\begin{aligned} I_{iii,\eta}^{(4)} &= -(3/35)I_\eta^{(0)} + (6/7)I_{ii,\eta}^{(2)}, & I_{iiij,\eta}^{(4)} &= (3/7)I_{ij,\eta}^{(2)}, \\ I_{iijj,\eta}^{(4)} &= (4/35)I_\eta^{(0)} - (1/7)I_{jj,\eta}^{(2)}, & I_{iijk,\eta}^{(4)} &= (1/7)I_{jk,\eta}^{(2)}. \end{aligned} \quad (8)$$

It has been shown previously that the third-order  $P_3$  spherical harmonic approximation yields significantly improved predictions compared the  $P_1$  closure.<sup>43</sup> This accuracy improvement however comes at the expense of a significant increase in computational cost. Moreover, higher-order approximations ( $N > 3$ ) of the hierarchy of spherical harmonic moment closures result in further substantial increases in computational efforts, whereas the accuracy improvements with increasing  $N$  are somewhat more modest.<sup>44,45</sup> For these reasons, it is felt that the  $P_3$  approximation provides a reasonable balance between accuracy and computational costs, relative to its higher- or lower-order counterparts.

### III.D. Maximum-Entropy $M_N$ Moment Closures

Among the infinite family of possible distributions that can be used to approximate the underlying distribution of the radiative intensity, the most probable form of the latter is given, according to Jaynes,<sup>18</sup> by the distribution that maximizes the radiative entropy,  $H_R(I_\eta)$ , subject to the constraints that a finite set of its angular moments,  $I_\eta^{(n)}$ ,  $n = 0, \dots, N$ , is known. The problem of finding such a distribution can be formulated in mathematical terms as follows:

$$\begin{aligned} \mathcal{I}_\eta &= \arg \max_{I_\eta} H_R(I_\eta) \\ \text{s.t. } \quad &\langle \vec{s}^{(n)} I_\eta \rangle = I_\eta^{(n)}, \quad n = 0, \dots, N, \end{aligned} \quad (9)$$

where  $N$  is the order of the highest moment in the closed system of moment equations and

$$H_R(I_\eta) = \langle h_R \rangle = \int_{4\pi} h_R(I_\eta) d\Omega, \quad (10)$$

and where  $h_R$  denotes the radiative entropy density, which, for combustion applications, corresponds to the entropy of radiation obeying Bose-Einstein statistics<sup>46</sup> and is given by

$$h_R(I_\eta) = \frac{2k\eta^2}{c} [(n+1) \ln(n+1) - n \ln(n)], \quad n = \frac{I_\eta}{2hc\eta^3}. \quad (11)$$

In Eq. (11),  $n$  is the occupation number, and  $h$  and  $k$  are the Planck and Boltzmann constants, respectively. The Lagrangian of the optimization problem given in Eq. (9) is

$$\mathcal{L}(I_\eta, \boldsymbol{\alpha}) = H_R(I_\eta) - \boldsymbol{\alpha}^T (\langle \mathbf{m}(\vec{s}) I_\eta \rangle - \mathbf{E}_\eta), \quad (12)$$

where  $\mathbf{E}_\eta$  is a vector containing all the independent entries of  $I_\eta^{(n)}$ ,  $n = 0, \dots, N$ ,  $\mathbf{m}(\vec{s})$  is a vector containing all the independent entries of  $\vec{s}^{(n)}$ ,  $n = 0, \dots, N$ , and  $\boldsymbol{\alpha}$  is the vector of Lagrange multipliers associated with the moment constraints. For a given finite set of angular moments, with associated Lagrange multipliers,  $\boldsymbol{\alpha}$ , the form of the entropy maximizing distribution can be derived via the stationary point of the Lagrangian, Eq. (12), i.e.,  $\partial \mathcal{L}(I_\eta, \boldsymbol{\alpha}) / \partial I_\eta = 0$ , which yields the following expression<sup>17</sup>

$$\mathcal{I}_\eta(\boldsymbol{\alpha}, \mathbf{m}) = 2hc\eta^3 \left[ \exp \left( \frac{c^2 h \eta}{k} \boldsymbol{\alpha}^T \mathbf{m}(\vec{s}) \right) - 1 \right]^{-1}. \quad (13)$$

In Eq. (13), the radiative intensity distribution is expressed in terms of the Lagrange multipliers,  $\boldsymbol{\alpha}$ , which depend on the angular moments of the distribution,  $\mathbf{E}_\eta$ . With the exception of the gray  $M_1$  closure,<sup>17</sup> there exist no analytical expressions for the Lagrange multipliers in terms of the known lower-order angular moments. The former must therefore be determined numerically in terms of the latter by solving the Lagrangian dual optimization problem

$$\max_{\boldsymbol{\alpha}} \{ \mathcal{L}^*(\boldsymbol{\alpha}) \}, \quad (14)$$

where  $\mathcal{L}^*(\boldsymbol{\alpha})$  is the Legendre transform of  $\mathcal{L}(I_\eta, \boldsymbol{\alpha})$ , Eq. (12), and has the form

$$\mathcal{L}^*(\boldsymbol{\alpha}) = \frac{2k\eta^2}{c} \left\langle \log \left[ \exp \left( \frac{c^2 h \eta}{k} \boldsymbol{\alpha}^T \mathbf{m}(\vec{s}) \right) - 1 \right] \right\rangle - \boldsymbol{\alpha}^T \mathbf{E}_\eta. \quad (15)$$

The wavenumber variable within the exponential term of Eq. (15) is rather inconvenient, since the Lagrange multipliers must then be solved not only for realizable sets of moments up to first-order, but also for values of wavenumber spanning the semi-infinite interval  $[0, +\infty]$ . A more convenient form for the optimization problem for entropy maximization, Eqs. (14) and (15), for the purpose of the proposed interpolation procedure, can however be obtained by the change of variables  $\boldsymbol{\beta} = (c^2 h \eta) \boldsymbol{\alpha} / k$ , such that

$$\begin{aligned} \mathcal{L}^*(\boldsymbol{\beta}) &= \left\langle \log \left[ \exp \left( \boldsymbol{\beta}^T \mathbf{m}(\vec{s}) \right) - 1 \right] \right\rangle - \boldsymbol{\beta}^T \mathbf{E}_\eta^*, \\ \mathcal{L}^*(\boldsymbol{\alpha}) &= 2ck\eta^2 \mathcal{L}^*(\boldsymbol{\beta}), \end{aligned} \quad (16)$$

where

$$\mathbf{E}_\eta^* = \frac{\pi \mathbf{E}_\eta}{C_1 \eta^3} = \{I_\eta^{(0)*}, I_\eta^{(1)*}, \dots\}, \quad I_\eta^{(n)*} = \frac{\pi I_\eta^{(n)}}{C_1 \eta^3}, \quad (17)$$

represents the set of angular moments up to order  $N$  used for the solution of the dual optimization problem, Eq. (16), and  $C_1 = 2\pi h c^2$  is the so-called first radiation constant. It is clear from Eq. (16) that, for any given wavenumber,  $\eta$ , maximizing  $\mathcal{L}^*(\boldsymbol{\alpha})$  is equivalent to maximizing  $\mathcal{L}^*(\boldsymbol{\beta})$ . Furthermore, the form given in the latter equation allows the parameterization of the Lagrange multipliers in terms of the ratio  $I_\eta^{(0)}/\eta^3$ , instead of  $I_\eta^{(0)}$  and  $\eta$ , separately, and this parameterization yields a reduction in the number of independent variables for the interpolation procedure of the non-gray  $M_2$  closure, which will be described in the sections to follow.

### III.E. Numerical Solution of the Optimization Problem for Entropy Maximization

The entropy of radiation based on Bose-Einstein statistics, given in Eq. (11), is a strictly convex functional, and, as such, any locally optimal set of Lagrange multipliers,  $\boldsymbol{\alpha}$ , for the dual optimization problem, Eq. (14), would also be a globally optimal set for the latter. The sequential quadratic programming (SQP) algorithm, as implemented in the software package NLOpt,<sup>47–49</sup> an open source library for nonlinear optimization, was therefore used for the numerical solution of the dual maximum entropy problem, Eq. (14). In this implementation, an objective function and its gradients, as well as constraints on the Lagrange multipliers so as to ensure non-negativity of the entropy maximizing distribution, Eq. (13), are supplied by the user. The Hessian matrix of second derivatives, which is required for solving the Newton system of equations at each iteration, is then estimated by means of the Broyden-Fletcher-Goldfarb-Shanno (BFGS) algorithm, which provides substantial computational savings compared to the direct evaluation of the Hessian matrix at every iteration.

The algorithm described above provides very good convergence for sets of moments far away from the boundaries of the realizability domain. However, as one of the boundaries is approached, the dual optimization problem becomes increasingly difficult to solve and might even fail to converge due to ill-conditioning of the Hessian matrix. In order to improve the condition number of the latter, a preconditioning procedure, similar to that described by Alldredge *et al.*,<sup>50</sup> is advocated. The preconditioning is equivalent to an adaptive change of polynomial basis for the angular moments, relative to the original monomial basis,  $\mathbf{m}(\vec{s})$ , such that the Hessian is the identity matrix in the new basis. In addition, the regularization scheme introduced by Alldredge *et al.*,<sup>51</sup> to make the optimization algorithm more robust, especially for very ill-conditioned problem, is also adopted. As an alternative to the Cholesky factorization of the Hessian for the preconditioning adopted by Alldredge *et al.*,<sup>50</sup> the modified Gram-Schmidt algorithm, described by Abramov,<sup>52</sup> is adopted. Furthermore, instead of preconditioning the Hessian matrix at each Newton step of the entropy optimization process, the procedure developed by Abramov,<sup>53</sup> allowing for several Newton steps between successive reorthogonalizations, is applied. The procedure consists of tracking the condition number of the inverse of the Hessian during the BFGS iterations, and then preconditioning the Hessian matrix whenever the condition number exceeds a threshold value of 20.

## IV. First-Order Maximum-Entropy $M_1$ Moment Closure for Non-Gray Gas

As an alternative to the first-order spherical harmonic,  $P_1$ , moment closure, the system of transport equations for angular moments up to first-order can be closed by assuming an entropy maximizing distribution with known angular moments up to first-order. The reconstructed approximate form of the distribution can then be integrated, with the appropriate angular weights, to obtain the second-order moments,  $I_\eta^{(2)\star}$  (see Eq. (17)), in terms of the lower-order moments, i.e.,  $I_\eta^{(2)\star} = I_\eta^{(2)\star}(I_\eta^{(0)\star}, I_\eta^{(1)\star})$ . Such a procedure results in the so-called first-order maximum-entropy,  $M_1$ , moment closure, which can be expressed in the so-called Eddington form as follows<sup>54</sup>

$$N^{(2)} = \frac{1 - \chi_2}{2} \vec{I} + \frac{3\chi_2 - 1}{2} \vec{n} \otimes \vec{n}, \quad I_\eta^{(2)\star} = N^{(2)} I_\eta^{(0)\star}, \quad (18)$$

where  $\vec{I}$  is the identity matrix,  $\vec{n} = N^{(1)} / \|N^{(1)}\|$  is the unit vector in the direction of the vector of first-order normalized moments,  $N^{(1)}$ , and  $\chi_2$  is the so-called Eddington factor, which is the only unknown in Eq. (18). Unlike the case of the  $M_1$  closure for a gray gas, there exists no exact analytical expression for the Eddington factor for a non-gray gas, which must therefore be determined numerically by solving the relatively expensive optimization problem for entropy maximization, Eqs. (14) and (16), for any given realizable set of moments up to first-order. For the purpose of radiation calculations in real gases, following the original development of the non-gray  $M_1$  closure by Sarr *et al.*,<sup>30</sup> an efficient and realizable interpolative-based approximation of the the Eddington factor has been recently developed by Sarr and Groth,<sup>31</sup> which results in a hyperbolic system of moment equations up to first order.

## V. Second-Order $M_2$ Maximum-Entropy Moment Closure for Non-Gray Gas

The primary focus of the present study is the next member of the hierarchy of maximum entropy closures, i.e., the second-order,  $M_2$ , moment closure. The latter provides closing relations to the system of moment equations up to second-order via reconstruction of an entropy maximizing distribution in terms of its known angular moments up to order two. The third-order angular moments,  $I_\eta^{(3)}$ , which correspond to the fluxes of the transport equations for the second-order angular moments, can then be expressed in terms of the known moments, i.e.,  $I_\eta^{(3)\star} = I_\eta^{(3)\star}(I_\eta^{(0)\star}, I_\eta^{(1)\star}, I_\eta^{(2)\star})$  (see Eq. (17)). Unfortunately, as mentioned in the previous section, it is not possible to obtain closed-form analytical expressions for the closing moment fluxes for the  $M_N$  closures, to the exception of the Bose-Einstein-based  $M_1$  closure for a gray medium. As such, in the context of real-gas radiation, repeated numerical solution of the optimization problem for entropy maximization, given by Eqs. (14) and (16), would therefore be necessary, whenever an update of the radiation solutions is required, making the application of the closure computationally expensive.

To circumvent the need for the costly solutions of the optimization problem to determine the Lagrange multipliers defining the maximum entropy distribution, an alternative interpolative-based approach for accurately approximating pre-computed values of the closing fluxes for the non-gray  $M_2$  closure is proposed herein. This approximation, in addition to attempting to retain some of the desirable properties of the original model (e.g., hyperbolicity of the moment equations), also results in substantially reduced computational costs compared to the repeated solution of the optimization problem for entropy maximization. The proposed interpolation procedure for the non-gray  $M_2$  closure is a direct extension of the framework adopted by Sarr and Groth<sup>24,25</sup> for the development of an interpolative-based approximation of the  $M_2$  closure in the case of gray radiation, which was motivated by the work of Pichard *et al.*,<sup>23</sup> who appear to be the first to develop interpolative-based approximations of the third-order closing fluxes for the gray  $M_2$  closure. It is formulated so as to closely match the form of the non-gray  $M_2$  maximum entropy solutions over the entire space of physically realizable moments up to second-order (i.e., the space defined by the set of necessary and sufficient conditions such that there exists a non-negative distribution reproducing moments up to second order). More specifically, a procedure based on affine combinations of the known analytical expressions of the third-order closing fluxes,  $N^{(3)}$ , on some of the boundaries of the realizable space for the second-order angular moments, is adopted to provide approximations for the closing fluxes of the non-gray  $M_2$  closure. The interpolants are chosen such that known analytical expressions of the third-order closing fluxes in the isotropic and the free-streaming limits, as well as on the boundaries of the realizable space for the second-order moments, are exactly reproduced. In the interior of the realizable space for the  $M_2$  closure, the interpolants also exactly reproduce pre-computed numerical maximum entropy solutions at a finite set

of points, chosen to coincide with roots or extrema of suitably selected orthogonal polynomials, which are known to provide quasi-optimal approximation to a function.

While the assumption of gray radiation was invoked in the study by Sarr and Groth,<sup>24,25</sup> non-gray participating media are of interest in the present study, which also involve the dependencies of the third-order closing fluxes on the radiative energy density and wavenumber. For the treatment of such additional dependencies, an extension of the procedure presented in the authors' recent paper,<sup>31</sup> in the context of the non-gray  $M_1$  closure, is adopted. In particular, an exponential mapping of the radiative energy density,  $I_\eta^{(0)*}$ , is employed for the purpose of our polynomial interpolation procedure, and the length scale of the mapping is systematically chosen so as to optimize the accuracy with respect to numerical maximum entropy solutions, while resulting in an overall hyperbolic closed system of moment equations up to second-order. However, unlike the procedure followed by Sarr and Groth,<sup>31</sup> realizability of the closing fluxes is not considered herein for the determination of the distribution of the length scale of the exponential mapping, due to the lack of necessary and sufficient conditions for realizability of angular moments up to third-order.

The development and description of the proposed interpolative-based non-gray second-order  $M_2$  closure are given below in the section to follow. More specifically, after a brief overview of the realizable space for angular moments up to second-order, an in-depth description of the theoretical details of the interpolative procedure for the non-gray  $M_2$  closure is carried out. Hyperbolicity of the resulting closed system of partial differential equations for the angular moments is discussed later in section VII.B.

### V.A. Interpolative-Based Second-Order $M_2$ Non-gray Maximum-Entropy Moment Closure

For angular moments up to second-order associated with an every-where non-negative angular distribution of the radiative intensity, the corresponding necessary and sufficient conditions on moment realizability, in multiple space dimensions, have been established by Kershaw,<sup>55</sup> and were recently revisited by Sarr and Groth.<sup>25</sup> Such conditions, which describe the realizable space for angular moments up to second order,  $\mathcal{R}^{(2)}$ , can be summarized as follows

$$\begin{aligned} \mathcal{R}^{(2)} = \{ & (I_\eta^{(0)}, I_\eta^{(1)}, I_\eta^{(2)}) \in \mathbb{R}^3 \times \mathbb{R}^{3 \times 3}, \quad \text{s.t.} \quad I_\eta^{(0)} \geq 0, \quad \|N^{(1)}\| \leq 1, \\ & N^{(2)} - N^{(1)}(N^{(1)})^T \geq 0, \quad \vec{n}^T N^{(2)} \vec{n} \leq 1 \quad \forall \quad \|\vec{n}\| \leq 1, \\ & \text{tr}(N^{(2)}) = 1 \quad \text{and} \quad N_{ij}^{(2)} = N_{ji}^{(2)} \}. \end{aligned} \quad (19)$$

One of the key steps in the proof of sufficiency of the above conditions is the transformation which sends the Cartesian axes in the coordinate frame where the covariance matrix,  $(N^{(2)} - N^{(1)}(N^{(1)})^T)$ , is diagonal, i.e., Cartesian axes aligned with principal axes of the covariance matrix. Such a transformation can be summarized as follows

$$\begin{aligned} \mathbb{T} : & (I_\eta^{(0)}, I_\eta^{(1)}, I_\eta^{(2)}) \rightarrow (I_\eta^{\prime(0)}, I_\eta^{\prime(1)}, I_\eta^{\prime(2)}) \\ \text{s.t.} & (N^{\prime(2)} - N^{\prime(1)}(N^{\prime(1)})^T) \quad \text{is diagonal positive definite,} \end{aligned} \quad (20)$$

where  $I_\eta^{\prime(i)}$ ,  $i = 0, \dots, 2$ , denote the images of the angular moments  $I_\eta^{(i)}$ ,  $i = 0, \dots, 2$ , under the rotational transformation which sends the coordinate axes along the principal axes of the covariance matrix. The latter can be expressed in terms of the former via the following relationships

$$I_\eta^{\prime(0)} = I_\eta^{(0)}, \quad I_{\eta,i}^{\prime(1)} = R_{ji} I_{\eta,j}^{(1)}, \quad I_{\eta,ij}^{\prime(2)} = R_{pi} R_{qj} I_{\eta,pq}^{(2)}, \quad (21)$$

where  $\mathbf{R}$  is the rotation matrix such that  $\mathbf{R}^T(N^{(2)} - N^{(1)}(N^{(1)})^T)\mathbf{R}$  is diagonal positive definite. Moreover, the third-order angular moments in the two coordinate systems can also be related as follows

$$I_{\eta,ijk}^{\prime(3)} = R_{li} R_{mj} R_{nk} I_{\eta,lmn}^{(3)}. \quad (22)$$

In Eq. (20), the quantities,  $N^{\prime(i)}$ ,  $i = 1, \dots, 2$ , represent normalized angular moments associated with the transformed full angular moments,  $I_\eta^{\prime(i)}$ ,  $i = 1, \dots, 2$ . In the new coordinate frame, the transformed second-order moment can be written as follows

$$N^{\prime(2)} = N^{\prime(1)}(N^{\prime(1)})^T + (1 - \|N^{\prime(1)}\|^2) \text{diag}(\gamma_1, \gamma_2, \gamma_3). \quad (23)$$

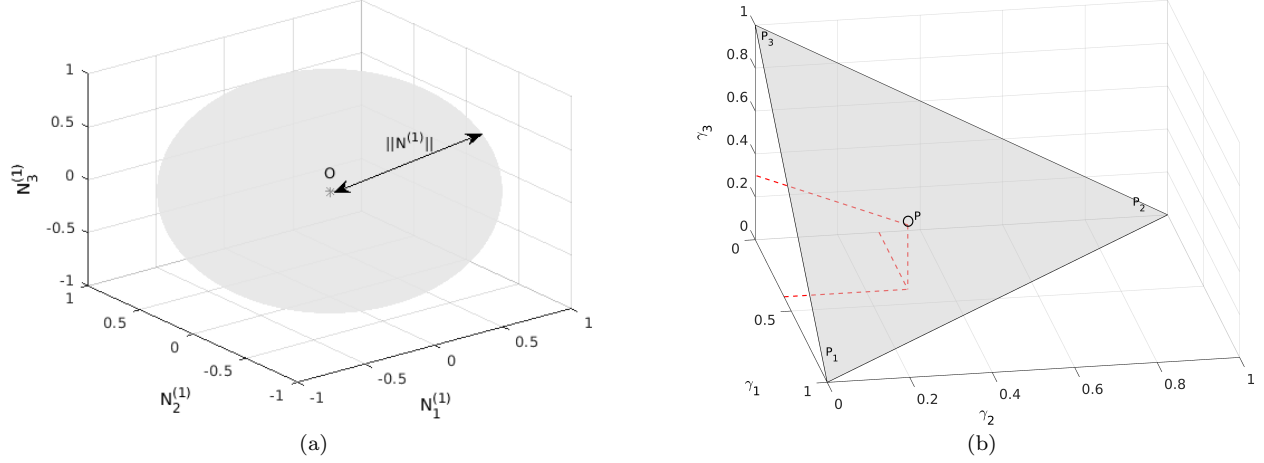


**Figure 1.** Realizability domain,  $\mathcal{R}_T^{(2)}$ , for the  $M_2$  closure in the frame where the covariance matrix,  $N^{(2)} - N^{(1)}(N^{(1)})^T$ , is diagonal positive definite for any given non-negative radiative energy density,  $I_\eta^{(0)}$ , and (a) a fixed set of normalized eigenvalues  $\{\gamma_1, \gamma_2, \gamma_3\}$ ; and (b) a fixed set of first-order moments  $\{N_1^{(1)}, N_2^{(1)}, N_3^{(1)}\}$ .

where  $\gamma_i$ ,  $i = 1 \dots 3$ , are the normalized eigenvalues of the covariance matrix, which satisfy the constraints  $\gamma_i \geq 0$  and  $\sum_{i=1}^3 \gamma_i = 1$ , and where the former constraint is a consequence of the positive semi-definiteness of the covariance matrix, whereas the latter equality stems from the trace equality on the covariance matrix. The realizability conditions in the new coordinate frame can then be summarized as follows

$$\mathcal{R}_T^{(2)} = \{(I_\eta^{(0)}, I_\eta^{(1)}, I_\eta^{(2)}) \in \mathbb{R} \times \mathbb{R}^3 \times \mathbb{R}^{3 \times 3}, \} \quad \text{s.t.} \quad I_\eta^{(0)} \geq 0, \quad \|N^{(1)}\| \leq 1, \quad (24)$$

$$0 \leq \gamma_i \leq 1, \quad i = 1 \dots 3, \quad \text{and} \quad \sum_{i=1}^3 \gamma_i = 1 \}.$$

The transformation which sends the Cartesian axes along the principal axes of the covariance matrix clearly allows for a more straightforward characterization of the realizable space for angular moments up to second order via a reduction of the number of independent variable from 9 to 6, in three-dimensional physical space. In fact, the set of angular moments up to second-order is represented by 9 independent variables since the zeroth-order moment,  $I_\eta^{(0)}$ , is a scalar, the first-order moment,  $I_\eta^{(1)}$ , is a 3-component vector, and the second-order moment,  $I_\eta^{(2)}$ , is a symmetric second-order dyad or tensor with 5 unique entries.

A graphical representation of the realizability domain for angular moments up to second-order,  $\mathcal{R}_T^{(2)}$ , is shown in Fig. 1, for any given non-negative radiative energy density,  $I_\eta^{(0)}$ . It can be clearly observed that for any given realizable first-order angular moment vector, the matrix of second order angular moments is realizable if and only if its normalized eigenvalues lie within the triangle  $(P_1, P_2, P_3)$ . At the vertices of the latter triangle, closed-form analytical expressions for the third-order angular moments,  $N^{(3)}$ , exist and are summarized in Table 1. We then aim to write the third-order closing fluxes for our non-gray  $M_2$  closure, for any given set of angular moments up to second-order in  $\mathcal{R}_T^{(2)}$ , as an affine interpolant of their known expressions at such vertices.

It is worth pointing out that the third-order normalized moment tensor,  $N^{(3)}$ , is symmetric and therefore

**Table 1.** Exact Analytic Expression of  $M_2$  Closing Relations at the Vertices of the Triangle  $(P_1, P_2, P_3)$ .

| Vertex | $N_{111}^{(3)}$  | $N_{122}^{(3)}$  | $N_{123}^{(3)}$                 |
|--------|--|--|---------------------------------|
| $P_1$  | $N_1^{(1)} \left[ (N_1^{(1)})^2 + (1 - \ N^{(1)}\ ^2) \right]$ | $N_1^{(1)} (N_2^{(1)})^2$                                      | $N_1^{(1)} N_2^{(1)} N_3^{(1)}$ |
| $P_2$  | $(N_1^{(1)})^3$  | $N_1^{(1)} \left[ (N_2^{(1)})^2 + (1 - \ N^{(1)}\ ^2) \right]$ | $N_1^{(1)} N_2^{(1)} N_3^{(1)}$ |
| $P_3$  | $(N_1^{(1)})^3$  | $N_1^{(1)} (N_2^{(1)})^2$                                      | $N_1^{(1)} N_2^{(1)} N_3^{(1)}$ |

**Table 2.** Form of the entropy maximizing distribution on the boundaries of the realizable space for angular moments up to second-order.

| Regime                             | Form of the Distribution  |
|------------------------------------|---|
| $\ N'^{(1)}\  = 1$                 | $I_\eta = I_\eta^{(0)} \delta(\vec{\Omega} - N'^{(1)})$   |
| $\gamma_i = 0$ or $\gamma_i = 1$   | see <sup>25</sup>   |
| $I_\eta^{(0)} \rightarrow 0$       | $\mathcal{I}_\eta(\boldsymbol{\alpha}, \mathbf{m}) = 2hc\eta^3 \exp\left(-\frac{c^2 h \eta}{k} \boldsymbol{\alpha}^T \mathbf{m}(\vec{s})\right)$                        |
| $I_\eta^{(0)} \rightarrow +\infty$ | $\mathcal{I}_\eta(\boldsymbol{\alpha}, \mathbf{m}) = \frac{2k\eta^2}{c} [\boldsymbol{\alpha}^T \mathbf{m}(\vec{s})]^{-1}$   |
| $int\mathcal{R}_T^{(2)}$           | $\mathcal{I}_\eta(\boldsymbol{\alpha}, \mathbf{m}) = 2hc\eta^3 \left[ \exp\left(\frac{c^2 h \eta}{k} \boldsymbol{\alpha}^T \mathbf{m}(\vec{s})\right) - 1 \right]^{-1}$ |

has just 10 unique, independent entries, in three-dimensional physical space. Furthermore, knowledge of just 3 of these entries, namely  $N'_{111}{}^{(3)}$ ,  $N'_{122}{}^{(3)}$  and  $N'_{123}{}^{(3)}$ , is sufficient to obtain values for the remaining 7 independent entries which can be related to these 3 entries as follows:

$$\begin{aligned}
 N'_{222}{}^{(3)}(I_\eta^{(0)*}, N_1^{(1)}, N_2^{(1)}, N_3^{(1)}, \gamma_1, \gamma_2) &= N'_{111}{}^{(3)}(I_\eta^{(0)*}, N_2^{(1)}, -N_1^{(1)}, N_3^{(1)}, \gamma_2, \gamma_1), \\
 N'_{333}{}^{(3)}(I_\eta^{(0)*}, N_1^{(1)}, N_2^{(1)}, N_3^{(1)}, \gamma_1, \gamma_2) &= N'_{111}{}^{(3)}(I_\eta^{(0)*}, N_3^{(1)}, N_2^{(1)}, -N_1^{(1)}, \gamma_3, \gamma_2), \\
 N'_{112}{}^{(3)}(I_\eta^{(0)*}, N_1^{(1)}, N_2^{(1)}, N_3^{(1)}, \gamma_1, \gamma_2) &= N'_{122}{}^{(3)}(I_\eta^{(0)*}, N_2^{(1)}, -N_1^{(1)}, N_3^{(1)}, \gamma_2, \gamma_1), \\
 N'_{113}{}^{(3)}(I_\eta^{(0)*}, N_1^{(1)}, N_2^{(1)}, N_3^{(1)}, \gamma_1, \gamma_2) &= N'_{122}{}^{(3)}(I_\eta^{(0)*}, N_3^{(1)}, N_1^{(1)}, N_2^{(1)}, \gamma_3, \gamma_1), \\
 N'_{133}{}^{(3)}(I_\eta^{(0)*}, N_1^{(1)}, N_2^{(1)}, N_3^{(1)}, \gamma_1, \gamma_2) &= N'_{122}{}^{(3)}(I_\eta^{(0)*}, N_1^{(1)}, N_3^{(1)}, -N_2^{(1)}, \gamma_1, \gamma_3), \\
 N'_{223}{}^{(3)}(I_\eta^{(0)*}, N_1^{(1)}, N_2^{(1)}, N_3^{(1)}, \gamma_1, \gamma_2) &= N'_{122}{}^{(3)}(I_\eta^{(0)*}, N_3^{(1)}, N_2^{(1)}, -N_1^{(1)}, \gamma_3, \gamma_2), \\
 N'_{233}{}^{(3)}(I_\eta^{(0)*}, N_1^{(1)}, N_2^{(1)}, N_3^{(1)}, \gamma_1, \gamma_2) &= N'_{122}{}^{(3)}(I_\eta^{(0)*}, N_2^{(1)}, N_3^{(1)}, N_1^{(1)}, \gamma_2, \gamma_3).
 \end{aligned} \tag{25}$$

It is also worth mentioning that the optimization problem for entropy maximization given by Eqs. (14) and (16) cannot be solved directly on the boundaries of the realizability domain,  $\mathcal{R}_T^{(2)}$ , denoted as  $\partial\mathcal{R}_T^{(2)}$ , and where some of the inequalities defining the realizable space,  $\mathcal{R}_T^{(2)}$ , become sharp, i.e.,

$$\begin{aligned}
 \partial\mathcal{R}_T^{(2)} = \{ & (I_\eta^{(0)}, I_\eta^{(1)}, I_\eta^{(2)}) \text{ s.t. } I_\eta^{(0)} \rightarrow 0 \text{ or } I_\eta^{(0)} \rightarrow +\infty \text{ or } \|N'^{(1)}\| = 1, \\
 & \text{or } \gamma_i = 0 \text{ or } \gamma_i = 1, \quad i \in \{1, 2, 3\} \}.
 \end{aligned} \tag{26}$$

In fact, on  $\partial\mathcal{R}_T^{(2)}$ , the entropy maximizing distribution of Eq. (13) becomes singular due to the fact that propagation of radiation is then only allowed along specific directions, instead of spanning the full solid angle. More specifically, the entropy maximizing distribution is either uniquely determined by a Dirac-delta distribution (for  $\|N'^{(1)}\| = 1$ ), or a combination of Dirac-delta distributions (for  $\gamma_i = 1$ ,  $i \in \{1, 2, 3\}$ , see<sup>25</sup>), or takes a particular form, as in the case of the limit where  $I_\eta^{(0)} \rightarrow 0$  or  $I_\eta^{(0)} \rightarrow +\infty$ , which are referred to as the hyperbolic and the logarithmic limits,<sup>56</sup> respectively. In the case where only one eigenvalue vanishes, i.e.,  $\gamma_i = 0$ ,  $i \in \{1, 2, 3\}$ , the distribution still has the form given in Eq. (13) for the entropy maximizing distribution, but is only defined over a circle instead of the full solid angle, as it becomes singular with respect to one of the direction cosines of the vector,  $\vec{s}$ , characterising the direction of propagation of radiation. The expressions for the entropy maximizing distribution associated with each of the aforementioned limits, are summarized in Table 2.

Based on the above, numerical maximum-entropy solutions for the third-order closing fluxes throughout the full realizable space,  $\mathcal{R}_T^{(2)} = int\mathcal{R}_T^{(2)} \cup \partial\mathcal{R}_T^{(2)}$ , can then be obtained by solving the optimization problem for entropy maximization using the appropriate form of the distribution for any given set of moments up to second order. We then aim to approximate the third-order closing fluxes at any point within  $\mathcal{R}_T^{(2)}$  by writing the entries,  $N'_{111}{}^{(3)} = N'_{111}{}^{(3)}(I_\eta^{(0)*}, N_1^{(1)}, N_2^{(1)}, N_3^{(1)}, \gamma_1, \gamma_2)$ ,  $N'_{122}{}^{(3)} = N'_{122}{}^{(3)}(I_\eta^{(0)*}, N_1^{(1)}, N_2^{(1)}, N_3^{(1)}, \gamma_1, \gamma_2)$  and  $N'_{123}{}^{(3)} = N'_{123}{}^{(3)}(I_\eta^{(0)*}, N_1^{(1)}, N_2^{(1)}, N_3^{(1)}, \gamma_1, \gamma_2)$ , as affine interpolants between their known closed-form expressions at the vertices of the triangle ( $P_1, P_2, P_3$ ) (see Table 1) as follows

$$N'_{111}{}^{(3)} = N_1^{(1)} \left[ (N_1^{(1)})^2 + f_{N'_{111}{}^{(3)}}(1 - \|N'^{(1)}\|^2) \right], \tag{27}$$

$$N'_{122}{}^{(3)} = N'_1{}^{(1)} \left( (N'_2{}^{(1)})^2 + f_{N'_{122}}{}^{(3)}(1 - \|N'{}^{(1)}\|^2) \right), \quad (28)$$

and

$$N'_{123}{}^{(3)} = f_{N'_{123}}{}^{(3)} N'_1{}^{(1)} N'_2{}^{(1)} N'_3{}^{(1)}, \quad (29)$$

where  $f_{N'_{111}}{}^{(3)} = f_{N'_{111}}{}^{(3)}(I'_\eta{}^{(0)\star}, N'_1{}^{(1)}, N'_2{}^{(1)}, N'_3{}^{(1)}, \gamma_1, \gamma_2)$ ,  $f_{N'_{122}}{}^{(3)} = f_{N'_{122}}{}^{(3)}(I'_\eta{}^{(0)\star}, N'_1{}^{(1)}, N'_2{}^{(1)}, N'_3{}^{(1)}, \gamma_1, \gamma_2)$ , and  $f_{N'_{123}}{}^{(3)} = f_{N'_{123}}{}^{(3)}(I'_\eta{}^{(0)\star}, N'_1{}^{(1)}, N'_2{}^{(1)}, N'_3{}^{(1)}, \gamma_1, \gamma_2)$  are polynomial expressions defined such that the proposed approximations of the third-order closing fluxes exactly match the known closed-form expressions at the vertices of the triangle,  $(P_1, P_2, P_3)$ , and consist of the following expressions

$$f_{N'_{111}}{}^{(3)} = \gamma_1 \left[ 1 + (1 - \gamma_1)g_{N'_{111}}{}^{(3)} \right], \quad (30)$$

$$f_{N'_{122}}{}^{(3)} = \gamma_2 \left[ 1 + \gamma_1 g_{N'_{122}}{}^{(3)} \right], \quad (31)$$

and

$$f_{N'_{123}}{}^{(3)} = 1 + \gamma_1 \gamma_2 \gamma_3 g_{N'_{123}}{}^{(3)}, \quad (32)$$

and where  $g_{N'_{111}}{}^{(3)} = g_{N'_{111}}{}^{(3)}(I'_\eta{}^{(0)\star}, N'_1{}^{(1)}, N'_2{}^{(1)}, N'_3{}^{(1)}, \gamma_1, \gamma_2)$ ,  $g_{N'_{122}}{}^{(3)} = g_{N'_{122}}{}^{(3)}(I'_\eta{}^{(0)\star}, N'_1{}^{(1)}, N'_2{}^{(1)}, N'_3{}^{(1)}, \gamma_1, \gamma_2)$ , and  $g_{N'_{123}}{}^{(3)} = g_{N'_{123}}{}^{(3)}(I'_\eta{}^{(0)\star}, N'_1{}^{(1)}, N'_2{}^{(1)}, N'_3{}^{(1)}, \gamma_1, \gamma_2)$  are polynomial expressions which are written as truncated series expansions in terms of orthogonal basis functions as follows

$$g_{N'_{uvw}}{}^{(3)} = \sum_{i=0}^{n_i} \sum_{j=0}^{n_j} \sum_{k=0}^{n_k} \sum_{l=0}^k \sum_{p=0}^{n_p} \sum_{q=0}^{n_p-p} C_{ijklpq}^{N'_{uvw}{}^{(3)}} T_i(\mathcal{M}_{I'_\eta{}^{(0)\star}}) T_{2j}(\|N'{}^{(1)}\|) Y_{2k}^{2l}(\theta, \phi) P_{pq}(\gamma_1, \gamma_2), \quad (33)$$

with  $n_i = n_j = n_k = n_p = 4$ .

In Eq. (33),  $T_n$  represents the Chebyshev polynomial of the first kind of degree  $n$ ,  $Y_k^l$  is the spherical harmonic function of degree  $k$  and order  $l$ ,  $P_{pq}$  represents the Proriol polynomial of order,  $p + q$ ,  $\theta$  and  $\phi$  respectively represent the polar and azimuthal angles characterizing the direction of the normalized first-order angular momentum vector,  $N'{}^{(1)}$ , in a spherical coordinate system and are defined as follows

$$\theta = \arccos \left( \frac{N'_3{}^{(1)}}{\|N'{}^{(1)}\|} \right), \quad \phi = \arccos \left( \frac{N'_1{}^{(1)}}{\sqrt{(N'_1{}^{(1)})^2 + (N'_2{}^{(1)})^2}} \right), \quad (34)$$

and  $\mathcal{M}_{I'_\eta{}^{(0)\star}}$  represents an exponential mapping of the radiative energy density, similar to the one adopted by Sarr and Groth,<sup>31</sup> of the form

$$\begin{aligned} \mathcal{M}_{I'_\eta{}^{(0)\star}} &: [0, +\infty] \rightarrow [-1, 1], \\ I'_\eta{}^{(0)\star} &\rightarrow 1 - 2 \exp \left( -\frac{I'_\eta{}^{(0)\star}}{L_{N'{}^{(3)}}} \right), \end{aligned} \quad (35)$$

and where  $L_{N'{}^{(3)}}$  is the length scale of the mapping,  $\mathcal{M}_{I'_\eta{}^{(0)\star}}$ , the distribution of which is chosen such that the accuracy of our interpolative-based approximations of the third-order closing fluxes, with respect to numerical maximum-entropy solutions, is optimized, for sets of angular moments up to second-order spanning  $\mathcal{R}_T^{(2)}$  and over the full spectrum of frequencies. The choice of the form of the mapping length scale is also dictated by some of the desirable properties of the original non-gray  $M_2$  closure, in particular hyperbolicity of the resulting closed system of moment equations. An in-depth description of the procedure adopted in the present study for determining the optimal distribution of  $L_{N'{}^{(3)}}$  is presented later in this section.

The coefficients,  $C_{ijklpq}^{N'_{uvw}{}^{(3)}}$ ,  $i = 0, \dots, n_i$ ,  $j = 0, \dots, n_j$ ,  $k = 0, \dots, n_k$ ,  $l = 0, \dots, k$ ,  $p = 0, \dots, n_p$ ,  $q = 0, \dots, n_p - p$ , appearing in Eq. (33), and defining the vector of coefficients,  $\mathbf{C}^{N'_{uvw}{}^{(3)}}$ , are determined via the solution of the Vandermonde system arising from the enforcement of the latter equation at several, suitably chosen, interpolation nodes spanning  $\mathcal{R}_T^{(2)}$ . In the present study, the interpolation points for  $\mathcal{M}_{I'_\eta{}^{(0)\star}}$  and

$\|N^{(1)}\|$  are chosen to coincide with extrema of Chebyshev polynomials of the first kind of order  $n_i$  and  $2n_j$ , respectively, including the endpoints. On the other hand, for the eigenvalues of the covariance matrix, a distribution similar to the one proposed by Blyth and Pozrikidis,<sup>57</sup> for the interpolation over the standard triangle, is employed, which yields

$$\gamma_{1,i} = \frac{1}{3}(1 + 2v_i - v_j - v_k), \quad \gamma_{2,j} = \frac{1}{3}(1 + 2v_j - v_i - v_k), \quad (36)$$

where  $i = 1, \dots, n_p + 1$ ,  $j = 1, \dots, n_p + 2 - i$ , and  $k = n_p + 3 - i - j$ , and where  $v_m$ ,  $m = 1, \dots, n_p + 1$ , are chosen to coincide with extrema of the shifted Chebyshev polynomial of the first kind of order  $n_p$ , also including the endpoints. The interpolation nodes for the polar angle  $\theta$  were chosen such that  $\cos \theta$  coincides with roots of the Legendre polynomials of order  $(2n_k + 1)$ , whereas, for the azimuthal angle,  $\phi$ , a set of  $4n_k$  points uniformly distributed on the unit circle were selected as the interpolation points. The choice of extrema of Chebyshev polynomials of the first kind, including the endpoints, also known as Chebyshev-Gauss-Lobatto points, for the purpose of interpolating over the domain spanned by the mapping,  $\mathcal{M}_{I_n^{(0)*}}$ , and the norm of the first-order normalized moment vector,  $\|N^{(1)}\|$ , as well as over the triangle  $(P_1, P_2, P_3)$ , allows for the derivatives of the third-order closing fluxes to be accurately reproduced in the isotropic ( $\|N^{(1)}\| = 0$ ) and the free-streaming ( $\|N^{(1)}\| = 1$ ) limits, as well as on the boundaries (edges) of the triangles of the triangle  $(P_1, P_2, P_3)$ , which correspond to situations where at least one of the eigenvalues of the covariance matrix vanishes. This feature is quite desirable as it ensures that our interpolative-based approximations of the third-order closing fluxes accurately capture the rates of change of the original maximum entropy solutions in such limits, and, consequently, oscillations of the interpolated solutions as such limits are approached, which can yield both realizability and hyperbolicity issues, are minimized. However, computations of the numerical values for  $g_{N'_{111}}^{(3)}$ ,  $g_{N'_{122}}^{(3)}$ , and  $g_{N'_{123}}^{(3)}$  from the maximum entropy solutions, using Eqs. (27) and (30) for  $N'_{111}^{(3)}$ , Eqs. (28) and (31) for  $N'_{122}^{(3)}$ , or Eqs. (29) and (32) for  $N'_{123}^{(3)}$ , respectively, for the purpose of solving the Vandermode system for the vector of coefficients,  $\mathbf{C}^{N'_{111}^{(3)}}$ ,  $\mathbf{C}^{N'_{122}^{(3)}}$ , and  $\mathbf{C}^{N'_{123}^{(3)}}$ , from Eq. (33), though straightforward for distributions away from the isotropic and free-streaming limits, as well as distributions away from the edges of the triangle described by the eigenvalues of the covariance matrix, result in undetermined expressions in these limits. In this study, l'Hopital's rule is used to provide computable expressions for  $g_{N'_{111}}^{(3)}$ ,  $g_{N'_{122}}^{(3)}$ , and  $g_{N'_{123}}^{(3)}$  in such limits, the derivation of which is not presented herein.

In the present study, the form of the length scale,  $L_{N'_{(3)}}$ , of the exponential mapping given in Eq. (35) is inspired from the expression proposed by Sarr and Groth,<sup>31</sup> in the case of the non-gray  $M_1$  closure, and can be seen as an extension of the latter to the case of known angular moments up to second-order. More specifically, we aim to write the length scale,  $L_{N'_{(3)}} = L_{N'_{(3)}}(N'_1{}^{(1)}, N'_2{}^{(1)}, N'_3{}^{(1)}, \gamma_1, \gamma_2)$  in the following form

$$L_{N'_{(3)}} = \exp \left[ \sum_{j=0}^{n_j} \sum_{k=0}^{n_k} \sum_{l=0}^k \sum_{p=0}^{n_p} \sum_{q=0}^{n_p-p} C_{jklpq}^{L_{N'_{(3)}}} T_{2j}(\|N^{(1)}\|) Y_{2k}^{2l}(\theta, \phi) P_{pq}(\gamma_1, \gamma_2) \right], \quad (37)$$

where the coefficients,  $C_{jklpq}^{L_{N'_{(3)}}}$ ,  $j = 0, \dots, n_j$ ,  $k = 0, \dots, n_k$ ,  $l = 0, \dots, k$ ,  $p = 0, \dots, n_p$ ,  $q = 0, \dots, n_p - p$ , defining the vector of coefficients,  $\mathbf{C}^{L_{N'_{(3)}}}$ , are chosen so as to accurately mimic numerical solutions of the entropy optimization problem, for the third-order closing fluxes, over the full realizable space for angular moments up to second order,  $\mathcal{R}_T^{(2)}$ , and over the full spectrum of frequencies. In the case of the non-gray  $M_1$  closure proposed by Sarr and Groth,<sup>31</sup> the determination of the coefficients for the length scale of the exponential mapping was only concerned with the Eddington factor, which is the only unknown in the second-order closing fluxes. In the present study, on the other hand, the optimal distribution of the length scale,  $L_{N'_{(3)}}$ , accounts simultaneously for the third-order closing fluxes  $N'_{111}^{(3)}$ ,  $N'_{122}^{(3)}$ , and  $N'_{123}^{(3)}$ , for which interpolative-based approximations are proposed herein. More specifically, the vector of coefficients,  $\mathbf{C}^{L_{N'_{(3)}}}$ , is computed herein via the solution of a nonlinear least-squares problem, which consists of minimizing a weighted sum of the  $L^2$  errors of the interpolative-based approximations of the third-order closing fluxes,

and can be summarized by the following expressions

$$\begin{aligned} & \min_{\mathbf{C}^{L_{N'}(3)}} \{ \text{weighted error}_{g_{N'_{uvw}}(3)} \}, \\ \text{weighted error}_{g_{N'_{uvw}}(3)} &= w_{N'_{111}}(3) \times \text{error}_{g_{N'_{111}}(3)} + w_{N'_{122}}(3) \times \text{error}_{g_{N'_{122}}(3)} + w_{N'_{123}}(3) \times \text{error}_{g_{N'_{123}}(3)}, \\ \text{error}_{g_{N'_{uvw}}(3)} &= \sum_{i=1}^{N_i} \sum_{j=1}^{N_j} \sum_{k=1}^{2N_k} \sum_{l=1}^{N_k} \sum_{p=1}^{N_p} \sum_{q=1}^{N_p-p} \sum_{r=1}^{N_r} w_i w_j w_k w_l w_{pq} w_r \left( g_{N'_{uvw},\text{fit}}^{ijklpqr} - g_{N'_{uvw},\text{numerical}}^{ijklpqr} \right)^2, \end{aligned} \quad (38)$$

where the weights,  $w_{N'_{111}}(3) = 0.4$ ,  $w_{N'_{122}}(3) = 0.3$ , and  $w_{N'_{123}}(3) = 0.3$ , respectively express the relative importance of each of the third-order closing fluxes,  $N'_{111}(3)$ ,  $N'_{122}(3)$ , and  $N'_{123}(3)$ , in the determination of the coefficients of the length of the exponential mapping of the radiative energy density.

In Eq. (38),  $g_{N'_{uvw},\text{numerical}}^{ijklpqr}$  represents values of the weighting function,  $g_{N'_{uvw}}(3)$ , of the affine interpolant given in Eq. (33), obtained via numerical solution of the optimization problem for entropy maximization for  $N = 2N_i N_j (N_k)^2 N_{pq} N_r = 6.72 \times 10^9$  evaluation points. The latter consist of  $N_i = 20$  values of  $\mathcal{M}_{I_\eta^{(0)*}}$  following a Gauss-Lobatto-Chebyshev distribution in  $[-1, 1]$ , with associated weights,  $w_i$ ,  $i = 1, \dots, N_i$ ,  $N_j = 20$  values of  $\|N^{(1)}\|$  associated with non-negative Gauss-Lobatto-Chebyshev points in  $[-1, 1]$ , with weighting  $w_j$ ,  $j = 1, \dots, N_j$ , and  $N_r = 100$  values of  $L_{N'}(3)$  based on roots of Laguerre polynomials with weighting  $w_r$ ,  $r = 1, \dots, N_r$ . Moreover,  $N_k = 20$  values of  $\theta$  and 40 values of  $\phi$  (see Eq. (34)) uniformly distributed in  $[0, \pi]$  and  $[0, 2\pi]$ , respectively, with weights,  $w_l$ ,  $l = 1, \dots, N_k$ , and  $w_k$ ,  $k = 1, \dots, 2N_k$ , were also used in the solution of the least-squares problem, in addition to  $N_{pq} = N_p(N_p + 1)/2 = 210$  points (with  $N_p = 20$ ) following the distribution given in Eq. (36), with associated weights,  $w_{pq}$ ,  $p = 1, \dots, N_p$ ,  $q = 1, \dots, N_p - p$ .

Furthermore, in Eq. (38),  $g_{N'_{uvw},\text{fit}}^{ijklpqr}$  corresponds to values of the weighting function,  $g_{N'_{uvw}}(3)$ , computed via evaluation of the proposed polynomial approximation, Eq. (33), at the test points. At each iteration of the nonlinear least-squares problem defined by Eq. (38), the iterate,  $\mathbf{C}^{L_{N'}(3)}$ , can be used, in conjunction with Eq. (37) as well as the inverse of the exponential mapping of Eq. (35), to compute values of  $I_\eta^{(0)*}$  associated with the chosen interpolation nodes for  $\mathcal{M}_{I_\eta^{(0)*}}$ , and consequently solve the corresponding dual maximum-entropy problem at each of the interpolation points. The vectors of coefficients,  $\mathbf{C}^{N'_{111}(3)}$ ,  $\mathbf{C}^{N'_{122}(3)}$ , and  $\mathbf{C}^{N'_{123}(3)}$  (see Eq. (33)), are then obtained via solution of the associated Vandermonde systems, and the resulting polynomial expressions of Eq. (33) are then used to compute the quantities,  $g_{N'_{111},\text{fit}}(3)$ ,  $g_{N'_{122},\text{fit}}(3)$ , and  $g_{N'_{123},\text{fit}}(3)$ , at the evaluation points.

Two equally important properties to consider for the purpose of our interpolation procedure, in addition to accuracy with respect to numerical maximum-entropy solutions for the third-order closing fluxes, are realizability and hyperbolicity of the interpolative-based non-gray  $M_2$  closure, throughout the full realizable space for angular moments up to second-order, in multiple space dimensions, as well as over the full spectrum of frequencies. Unfortunately, unlike the case for the non-gray  $M_1$  closure, necessary and sufficient conditions for realizability of angular moments up to third-order in multi-dimensional physical space are not available to date, and, as such, realizability of the third-order closing fluxes is not considered in the proposed interpolation procedure. On the other hand, hyperbolicity of our proposed non-gray  $M_2$  closure is sought by enforcing, at each step of the least-squares optimization problem, Eq. (38), appropriate constraints on the eigenvalues of the flux Jacobian of the resulting closed system of equations, as discussed in Section VII.B.

It should be pointed out that several improvements in our polynomial interpolation procedure have been made compared to the one adopted by Sarr and Groth<sup>25</sup> for the gray  $M_2$  closure, thereby resulting in improved efficiency of our interpolative-based approximations of the maximum-entropy-based third-order closing fluxes. First, instead of employing the rectangle-triangle mapping adopted by Sarr and Groth,<sup>25</sup> in conjunction with a product of Chebyshev polynomials, for the interpolation over the triangle,  $(P_1, P_2, P_3)$ , in this study, we make use of Prorior polynomials, which represent a complete set of orthogonal basis polynomials on the standard triangle, and result in a well-conditioned Vandermonde matrix when used in conjunction with the nodal distribution given in Eq. (36), for the interpolation over the triangle,  $(P_1, P_2, P_3)$ . Moreover, the latter nodal distribution, i.e., that of Eq. (36), provides a better distribution of interpolation nodes over the triangle, unlike the rectangle-triangle mapping employed by Sarr and Groth,<sup>25</sup> which unnecessarily and undesirably clusters the interpolation points near one of the vertices or edges of

the triangle. As for the spherical harmonic expansion in terms of the polar and azimuthal angles associated with the vector of first-order moments, a careful analysis of the evenness of the third-order closing fluxes revealed that only the spherical harmonic functions of even degree and even order need to be retained for the interpolations, instead of including all the terms, whether even or odd, in the expansion, as was done in.<sup>25</sup> Using these facts yields a reduction in the total number of coefficients for the interpolations by half, at least. The aforementioned improvements, despite resulting in a more efficient interpolative procedure for the third-order closing fluxes of the  $M_2$  closure, still yield a relatively computationally expensive closure for comparisons with the recently developed interpolative-based approximation of its lower-order counterpart,<sup>31</sup> the non-gray  $M_1$  closure, as well as the  $P_1$  and  $P_3$  spherical harmonic moment closures. In fact, the set of orthogonal polynomial bases, used for the interpolation of maximum entropy solutions, for the third-order closing fluxes, over the full realizable space for moments up to second-order, while very convenient for accurately computing the coefficients associated with our proposed polynomial approximations, Eq. (33), would involve repeated computations of factorial expressions, among others, when implemented directly for use in computing approximations to the entries of  $N^{(3)}$ . In light of this, substantial computational savings can be achieved by reformulating the polynomial expressions for  $g_{N'_{111}}^{(3)}$ ,  $g_{N'_{122}}^{(3)}$ , and  $g_{N'_{123}}^{(3)}$  (see Eq. (33)), as well as for  $L_{N^{(3)}}$  (see Eq. (37)), in terms of monomials with respect to the independent variables, once the coefficients,  $C^{N'_{111}}^{(3)}$ ,  $C^{N'_{122}}^{(3)}$ ,  $C^{N'_{123}}^{(3)}$ , and  $C^{L_{N^{(3)}}}$ , have been determined. The resulting polynomial interpolants, given in Eqs. (33) and (37), can then be evaluated very efficiently by means of the well known Horner scheme.<sup>58,59</sup>

## VI. Implementation of $M_2$ Closure with Narrow-Band Correlated- $k$ Model

The RTE, as defined in Eq. (1), represents the transport of radiation for a single wavenumber. In reactive flows however, the radiative properties of participating gases, in particular the absorption coefficient, varies strongly throughout the spectrum. The statistical narrow-band correlated- $k$  (SNBCK) model is employed in this study in order to treat such strong spectral dependence. In the SNBCK model, the spectral domain is divided into bands of frequencies of size  $\Delta\eta$ . The size of the bands is chosen to be sufficiently small such that the Planck function,  $I_{b\eta}$ , can be assumed to be constant within each band. A cumulative distribution function for the absorption coefficient,  $g(k)$ , which can be interpreted as a dimensionless wavenumber coordinate varying between 0 and 1, is then introduced. This cumulative distribution function allows the reordering of the strongly spectrally varying absorption coefficient into a monotonic function, such that the number of evaluations of the RTE, required for accurate integration over each narrow-band, is substantially reduced in comparison to straightforward line-by-line methods. Assuming a non-scattering medium, the RTE of Eq. (1), integrated over each narrow band, yields

$$\int_0^1 \frac{1}{c} \frac{\partial I_g}{\partial t} dg + \int_0^1 \vec{s} \cdot \vec{\nabla} I_g dg = \int_0^1 k(g)(I_{b\eta_c} - I_g) dg, \quad (39)$$

where

$$I_g = \frac{\int_{\Delta\eta} I_\eta \delta(k - \kappa_\eta) d\eta}{\int_{\Delta\eta} \delta(k - \kappa_\eta) d\eta} \quad (40)$$

and where  $I_{b\eta_c}$  is the Planck function evaluated at the wavenumber corresponding to the band centre, denoted herein by  $\eta_c$ . In the context of the statistical narrow-band correlated- $k$  model considered herein, the cumulative distribution function,  $g(k)$ , is obtained by taking the inverse Laplace transformation of the statistical narrow-band transmissivity,<sup>60</sup> the construction of which is based on the narrow-band data of Soufiani and Taine<sup>61</sup> for water vapour ( $H_2O$ ), carbon dioxide ( $CO_2$ ) and carbon monoxide ( $CO$ ). In order to achieve computational savings, the three radiating gases are approximated by a single gas with effective narrow-band parameters based on the optically thin limit.<sup>9</sup> In addition, the band lumping procedure described by Liu *et al.*<sup>8</sup> is also adopted, whereby several bands are combined to form wide bands. A total of nine non-uniformly spaced wide bands are employed herein based on the recommendation of Goutiere *et al.*<sup>62</sup>

The integration over the narrow-bands is performed by means of Gauss-Legendre quadrature, such that

the spectrally integrated intensity for each band is computed as

$$\overline{I_{\Delta\eta}} = \sum_{i=1}^{N_g} w_i I(g_i), \quad (41)$$

where  $N_g$  is the number of Gauss quadrature points and  $w_i$  are the weights. Liu *et al.*<sup>7</sup> found that four Gauss quadrature points provide a good balance between accuracy and computational costs. The divergence of the radiative heat flux, also referred to as the radiative source term, which is the quantity of interest in reactive flows simulations, is then evaluated as

$$S_R = \nabla \cdot \mathbf{q}_{rad} \approx \sum_{j=1}^{N_b} \sum_{i=1}^{N_g} w_i \kappa(g_i) (4\pi I_{b\eta c_j} - \langle I(g_i) \rangle) \Delta\eta_j, \quad (42)$$

where  $N_b$  is the number of narrow bands,  $\Delta\eta_j$  is the width of the  $j$ th narrow-band, and  $\langle I(g_i) \rangle$  represents the angular integral, more specifically the zeroth-order moment (see Eq. (3)), of the intensity distribution, and is obtained by solving the RTE at quadrature point  $g_i$ .

Using either the DOM or the  $P_N$  moment closures, an estimate of the radiative energy density,  $\langle I(g_i) \rangle$ , at each of the quadrature points,  $g_i$ , for use in Eq. (42), can be easily obtained. However, for the proposed non-gray  $M_2$  closure, coupling with the SNBCK presents additional challenges due to the explicit wavenumber dependence of the resulting closing relations, as was also the case for the non-gray  $M_1$  closure developed by Sarr *et al.*<sup>30</sup> and improved by Sarr and Groth.<sup>31</sup> Nevertheless, a close examination of the entropy maximizing distribution, Eq. (13), reveals that it has the same form as the Planck function, which reads as follows

$$I_{b\eta}(T) = 2hc\eta^3 \left[ \exp\left(\frac{hc\eta}{kT}\right) - 1 \right]^{-1}. \quad (43)$$

In fact, a close inspection of Eqs. (13) and (43) shows that the Planck function and the entropy maximizing distribution, for a given finite set of angular moments, only differ by the expressions in the respective exponential terms. More specifically, for any given wavenumber, the Planck function can be thought of as an isotropic distribution of the radiative intensity, while the entropy maximizing distribution allows departures from the equilibrium or isotropic distribution via the Lagrange multipliers. This suggests that, for the same energy density (zeroth-order moment), the entropy maximizing distribution has similar profiles, with respect to wavenumber, compared to the blackbody intensity, over the full spectrum of frequencies, except that the former is shifted relative to the latter in frequency space. It would therefore seem reasonable to evaluate the entropy maximizing distribution at the wavenumber corresponding to the band centre, similar to the Planck function, and such a procedure is adopted here, as was also done for the non-gray  $M_1$  closure recently proposed by the authors.<sup>30,31</sup>

## VII. Numerical Solution Method

Similar to the  $P_1$  and  $P_3$  moment closures, as well as the non-gray  $M_1$  interpolative closure of Sarr and Groth,<sup>31</sup> the proposed interpolative-based non-gray second-order maximum-entropy,  $M_2$ , moment closure is strictly hyperbolic in the sense of Lax.<sup>63</sup> While not proven here, strong numerical evidence for the hyperbolicity of the proposed  $M_2$  closure is provided here. In the original definition, quasi-linear inhomogeneous PDEs are said to be strictly hyperbolic if the eigenvalues associated with the eigensystem of the coefficient matrices and flux Jacobians are all real and distinct. A slightly less restrictive demand for strict hyperbolicity is that the eigenvalues are all real (i.e., repeated eigenvalues are permitted) and that the corresponding right eigenvectors form a complete and linearly independent set such that the coefficient matrices and flux Jacobians are diagonalizable. Levermore<sup>64</sup> has shown that the maximum-entropy closures applied to the Boltzmann equations of gas kinetic theory with the Boltzmann entropy result in moment equations that are symmetric hyperbolic systems and strictly hyperbolic.

Quasi-linear hyperbolic PDEs of the type governing the system of angular moments for the  $M_2$  closure are very well suited for solution by the now standard family of upwind finite-volume spatial discretization techniques originally developed by Godunov.<sup>65</sup> In this study, solutions of the proposed interpolative-based  $M_2$  closure for non-gray radiation, as well as those of the non-gray  $M_1$  closure, and the  $P_1$  and  $P_3$  moment

closures, are all obtained using a parallel, implicit, upwind Godunov-type finite-volume scheme similar to those previously described by Groth and co-workers<sup>1–6</sup> for systems of partial differential equations. In what follows, the proposed numerical solution methodology is described for the non-gray  $M_2$  moment closure. Similar solution procedures are also applied here for the non-gray  $M_1$  closure as well as the two  $P_N$  closure methods. Additionally, the hyperbolicity of the proposed interpolative-based  $M_2$  closure is explored by numerical means and discussed in Subsection VII.B below.

### VII.A. Weak Conservation Form of $M_2$ Moment Equations

The finite-volume scheme used in the numerical solution of the proposed interpolative-based non-gray second-order maximum entropy,  $M_2$ , moment closure considers the weak conservation form of the moment equations applied to two-dimensional, body-fitted, multi-block, quadrilateral meshes. The weak conservation form of the  $M_2$  moment equations for a two-dimensional Cartesian coordinate system can be obtained by taking appropriate angular moments of the underlying RTE for a non-gray medium and written as

$$\frac{\partial \mathbf{U}}{\partial t} + \frac{\partial \mathbf{F}}{\partial x} + \frac{\partial \mathbf{G}}{\partial y} = \mathbf{S}, \quad (44)$$

where  $\mathbf{U}$  is the vector of conserved moments given by

$$\mathbf{U} = \left[ I_g^{(0)}, I_{g,1}^{(1)}, I_{g,2}^{(1)}, I_{g,11}^{(2)}, I_{g,12}^{(2)}, I_{g,22}^{(2)} \right]^T, \quad (45)$$

$\mathbf{F}$  and  $\mathbf{G}$  are the flux vectors in the  $x$ - and  $y$ -coordinate directions, respectively, having the form

$$\begin{aligned} \mathbf{F} &= c \left[ I_{g,1}^{(1)}, I_{g,11}^{(2)}, I_{g,12}^{(2)}, I_{g,111}^{(3)}, I_{g,112}^{(3)}, I_{g,122}^{(3)} \right]^T, \\ \mathbf{G} &= c \left[ I_{g,2}^{(1)}, I_{g,12}^{(2)}, I_{g,22}^{(2)}, I_{g,211}^{(3)}, I_{g,212}^{(3)}, I_{g,222}^{(3)} \right]^T, \end{aligned} \quad (46)$$

and where  $\mathbf{S}$  represents the source term vector, which, under the assumption of isotropic scattering, is given by

$$\mathbf{S} = c \begin{bmatrix} k(g)(4\pi I_{b\eta_c} - I_g^{(0)}) \\ -(k(g) + \sigma_s)I_{g,1}^{(1)} \\ -(k(g) + \sigma_s)I_{g,2}^{(1)} \\ \frac{1}{3}(4\pi k(g)I_{b\eta_c} + \sigma_s I_g^{(0)}) - (k(g) + \sigma_s)I_{g,11}^{(2)} \\ -(k(g) + \sigma_s)I_{g,12}^{(2)} \\ \frac{1}{3}(4\pi k(g)I_{b\eta_c} + \sigma_s I_g^{(0)}) - (k(g) + \sigma_s)I_{g,22}^{(2)} \end{bmatrix}. \quad (47)$$

It is worth mentioning that the subscript,  $g$ , indicates a reordered quantity, from frequency space to the domain defined by the cumulative distribution function,  $g$ , and the following definition holds

$$I_g^{(n)}(\vec{x}, t) = \langle \vec{s}^n I_g(\vec{x}, \vec{s}, t) \rangle, \quad (48)$$

where the reordered intensity distribution,  $I_g$ , is defined in Eq. (40). The corresponding normalized angular moments in the reordered space are computed in a similar way as in Eq. (4), except that the wavenumber subscript is replaced by a subscript based on the cumulative distribution function,  $g$ . In Eq. (46), the third-order moment fluxes are related to the known lower-order moments through the expressions given in Eqs. (25), (27)–(33), defined above, thereby resulting in the non-gray  $M_2$  closure.

### VII.B. Eigenstructure And Hyperbolicity of Interpolative-Based Non-Gray $M_2$ Moment Closure

The hyperbolicity of the closed system of moment equations up to second order, resulting from the proposed interpolative-based approximation of the third-order closing fluxes for the non-gray  $M_2$  closure, in two space dimensions, is investigated by considering the eigenvalues of the flux Jacobian  $\mathbf{A} = \partial \mathbf{F} / \partial \mathbf{U}$  and  $\mathbf{B} = \partial \mathbf{G} / \partial \mathbf{U}$  for the  $x$ - and  $y$ -coordinate directions, respectively. Hyperbolicity is ensured if the eigenvalues

of the Jacobians  $\mathbf{A}$  and  $\mathbf{B}$  are all real. For the non-gray  $M_2$  closure, the flux Jacobian in the  $x$ -direction,  $\mathbf{A}$ , can be written as

$$\mathbf{A} = \frac{\partial \mathbf{F}}{\partial \mathbf{U}} = c \begin{bmatrix} 0 & 1 & 0 & 0 & 0 & 0 \\ 0 & 0 & 0 & 1 & 0 & 0 \\ 0 & 0 & 0 & 0 & 1 & 0 \\ \frac{\partial I_{g,111}^{(3)}}{\partial I_g^{(0)}} & \frac{\partial I_{g,111}^{(3)}}{\partial I_g^{(1)}} & \frac{\partial I_{g,111}^{(3)}}{\partial I_g^{(2)}} & \frac{\partial I_{g,111}^{(3)}}{\partial I_g^{(1,1)}} & \frac{\partial I_{g,111}^{(3)}}{\partial I_g^{(1,2)}} & \frac{\partial I_{g,111}^{(3)}}{\partial I_g^{(2,2)}} \\ \frac{\partial I_{g,112}^{(3)}}{\partial I_g^{(0)}} & \frac{\partial I_{g,112}^{(3)}}{\partial I_g^{(1)}} & \frac{\partial I_{g,112}^{(3)}}{\partial I_g^{(2)}} & \frac{\partial I_{g,112}^{(3)}}{\partial I_g^{(1,1)}} & \frac{\partial I_{g,112}^{(3)}}{\partial I_g^{(1,2)}} & \frac{\partial I_{g,112}^{(3)}}{\partial I_g^{(2,2)}} \\ \frac{\partial I_{g,122}^{(3)}}{\partial I_g^{(0)}} & \frac{\partial I_{g,122}^{(3)}}{\partial I_g^{(1)}} & \frac{\partial I_{g,122}^{(3)}}{\partial I_g^{(2)}} & \frac{\partial I_{g,122}^{(3)}}{\partial I_g^{(1,1)}} & \frac{\partial I_{g,122}^{(3)}}{\partial I_g^{(1,2)}} & \frac{\partial I_{g,122}^{(3)}}{\partial I_g^{(2,2)}} \end{bmatrix}, \quad (49)$$

where the derivatives of the third-order closing fluxes with respect to the lower-order angular moments making up the components of the solution vector,  $U_q$ ,  $q = 1, \dots, 6$  (see Eq. (45)), in  $\mathcal{R}^{(2)}$ , can be written, using the product rule, in conjunction with the inverse of the relationship given in Eq. (22), in the form

$$\frac{\partial I_{g,ijk}^{(3)}}{\partial U_q} = I'_{g,lmn}{}^{(3)} \frac{\partial}{\partial U_q} (R_{il}R_{jm}R_{kn}) + R_{il}R_{jm}R_{kn} \frac{\partial I'_{g,lmn}{}^{(3)}}{\partial U_q}. \quad (50)$$

Further applying the product rule on the derivatives appearing in the first term on the right hand side of the latter equation allows us to write

$$\frac{\partial}{\partial U_q} (R_{il}R_{jm}R_{kn}) = R_{jm}R_{kn} \frac{\partial R_{il}}{\partial U_q} + R_{il}R_{kn} \frac{\partial R_{jm}}{\partial U_q} + R_{il}R_{jm} \frac{\partial R_{kn}}{\partial U_q}. \quad (51)$$

To further decompose the derivatives involved in the second term on the right hand side of Eq. (50), we make use of the chain rule of derivatives, which when combined with the application of the product rule on the relationship,  $U'_i = T_{ij}U_j$ , yields the following expression

$$\frac{\partial I'_{g,lmn}{}^{(3)}}{\partial U_q} = \frac{\partial I'_{g,lmn}{}^{(3)}}{\partial U'_p} \left( T_{pq} + U_r \frac{\partial T_{pr}}{\partial U_q} \right), \quad (52)$$

where  $\mathbf{T}$  represents the rotation matrix which transforms the components of the vector of conserved variables,  $\mathbf{U}$ , in  $\mathcal{R}^{(2)}$ , into the elements of the vector of conserved variables,  $\mathbf{U}'$ , in  $\mathcal{R}_T^{(2)}$ .

Analytical expressions for the derivatives of the closing fluxes  $I'_{ijk}{}^{(3)}$ , in  $\mathcal{R}_T^{(2)}$ , with respect to the lower-order moments,  $U'_q$ , in  $\mathcal{R}_T^{(2)}$ , can be readily derived by using Eqs. (25), (27)-(33). Furthermore, the derivatives appearing in Eq. (51) can also be obtained from the analytical form of the rotation matrix,  $\mathbf{R}$ , with respect to the lower-order moments,  $U_q$ ,  $q = 1, \dots, 6$ , in  $\mathcal{R}^{(2)}$ .

In order to ensure hyperbolicity of the system of equations resulting from our proposed interpolative non-gray  $M_2$  closure, constraints on the eigenvalues of the flux Jacobian of Eq. (49), such that the latter are real, are enforced, at every step of the non-linear least-squares optimization problem, Eq. (38), for each of the sample points used to assess the error given in the latter equation.

The numerical solution of the non-linear least-squares problem, Eq. (38), in conjunction with the constraints of hyperbolicity discussed above, yields a distribution of the length scale,  $L_{N'}{}^{(3)}$  (see Eq. (37)), of the exponential mapping for which the eigenvalues of the flux Jacobian,  $\mathbf{A}$ , are all real valued for all of the test points considered within the space of realizable moments up to second order. Due to the geometric symmetries of the closure, similar findings are expected for the  $y$ -direction flux Jacobian,  $\mathbf{B}$ . It should be pointed out that the above numerical findings are certainly not a proof that the eigenvalues are everywhere real nor was the issue of strict hyperbolicity tested as part of this study. In particular, it was indeed felt that the distinct nature of the eigenvalues and/or non-degenerate nature of the eigenstructure can be difficult to confirm by numerical means. Nevertheless, the local hyperbolicity of the proposed interpolative-based non-gray  $M_2$  closure for all points examined within the space of physically realizable moments is very encouraging and provides strong evidence of the extent to which the proposed interpolative-based closure mimics the actual non-gray second-order,  $M_2$ , maximum-entropy model, which of course is known to be hyperbolic.

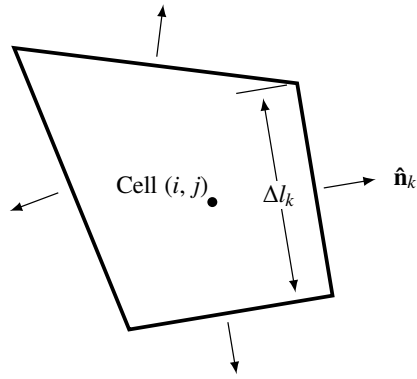


Figure 2. Quadrilateral computational cell of two-dimensional multi-block body-fitted mesh.

### VII.C. Finite-Volume Spatial Discretization Procedure and Semi-Discrete Form

In the proposed second-order limited upwind finite-volume method, the integral form of the conservation equations defined by Eq. (44) is applied to quadrilateral cells of a two-dimensional multi-block body-fitted grid. This results in the so-called semi-discrete form, a coupled system of nonlinear ordinary differential equations for cell-averaged solution quantities, which can be written for computational cell  $(i, j)$  (see Fig. 2) as

$$\frac{d\mathbf{U}_{i,j}}{dt} = -\frac{1}{A_{i,j}} \sum_{m=1}^{N_f} \vec{\mathbf{F}}_{i,j,m} \cdot \vec{n}_{i,j,m} \Delta l_{i,j,m} + \mathbf{S}_{i,j}(\mathbf{U}_{i,j}) = -\mathbf{R}_{i,j}(\mathbf{U}), \quad (53)$$

where  $\mathbf{U}_{i,j} = (1/A_{i,j}) \int_{A_{i,j}} \mathbf{U} dA$  is the cell-averaged conserved solution vector,  $\vec{\mathbf{F}} = [\mathbf{F}, \mathbf{G}]$  is the moment flux dyad,  $\mathbf{R}_{i,j}(\mathbf{U})$  is the residual vector,  $A_{i,j}$  is the cell surface area,  $\Delta l_{i,j,m}$  and  $\vec{n}_{i,j,m}$ , respectively, are the length and unit outward normal vector of the  $m^{\text{th}}$  face of quadrilateral cell  $(i, j)$  having  $N_f = 4$  cell faces.

### VII.D. Numerical Flux Evaluation

The numerical moment flux,  $\vec{\mathbf{F}} \cdot \vec{n}$ , at cell faces,  $(i, j, m)$ , appearing in the semi-discrete form of the moment equations given in Eq. (53) above are evaluated here using a Riemann solver-based flux function in conjunction with piecewise limited linear reconstruction. In this approach, the numerical moment flux can be expressed as

$$\vec{\mathbf{F}} \cdot \vec{n} = \mathcal{F}(\mathbf{U}_L, \mathbf{U}_R, \vec{n}), \quad (54)$$

where  $\mathcal{F}$  is the so-called numerical flux function and  $\mathbf{U}_L$  and  $\mathbf{U}_R$  are respectively the values of solutions at the mid-point of the cell face to the left (inside the cell) and right (outside the cell) of the interface. The widely-used HLLC approximate Riemann solver, based on the approximate Riemann solver of Harten, Lax, and van Leer<sup>66</sup> with estimates of the wave speeds due to Einfeldt<sup>67</sup> is used here to define the flux function,  $\mathcal{F}$ . Piecewise limited linear reconstruction based on the least-squares approach of Barth<sup>68</sup> with the slope limiter of Venkatakrishnan<sup>69</sup> to ensure solution monotonicity are used to reconstruct the values of  $\mathbf{U}_L$  and  $\mathbf{U}_R$  at the cell interfaces.

### VII.E. Block-Based Anisotropic Adaptive Mesh Refinement (AMR)

While not applied in the present study, the finite-volume scheme described above can also be used in conjunction with a block-based hierarchical data structure to facilitate automatic solution-directed mesh adaptation on multi-block mesh according to physics-based criteria. The block-based anisotropic AMR implemented here is similar to that described by Groth and co-workers<sup>70–73</sup> for computations of two-dimensional problems and<sup>71,73–75</sup> for three-dimensional flows. The anisotropic approach allows the adaptation of the mesh based on solution-dependent physics-based criteria as the computation is performed, such that areas associated with small spatial scales (e.g., regions with shocks, steep gradients, and/or discontinuities) are resolved with appropriately higher mesh densities, while areas with larger spatial scales are resolved on coarser meshes associated with large cell sizes. The block-based anisotropic AMR scheme has been shown to be very effective

in reducing the overall mesh size for a given flow problem as well as providing efficient and highly scalable implementation on high-performance parallel computing systems using domain decomposition.<sup>4,73,75,76</sup>

### VII.F. Newton Krylov Schwarz (NKS) Method

In most practical applications involving radiative heat transfer, the time scales for the transport of the radiation are generally much smaller than those associated with the other phenomena involved, thereby making steady-state solutions of the RTE of primary interest. Newton’s method is applied herein to obtain, in an efficient manner, steady-state solutions of the algebraic non-linear equations following from Eq. (53) and satisfying

$$\mathbf{R}(\mathbf{U}) = -\frac{d\mathbf{U}}{dt} = \mathbf{0}. \quad (55)$$

The particular implementation of the Newton method used here has been developed previously by Groth and Northrup<sup>77</sup> as well as Charest *et al.*<sup>5,78</sup> for computations on large multi-processor parallel clusters. It consists of a Jacobian-free inexact Newton method coupled with an iterative Krylov subspace linear solver. The widely-used generalized minimal residual (GMRES) technique developed by Saad and co-workers<sup>79–82</sup> is used to solve the linear system at each Newton step. The technique is particularly attractive because the left-hand-side matrix of the linear system is not explicitly formed and instead only the results of matrix-vector products are required at each iteration, thereby significantly reducing the required storage. A combination of additive Schwarz and block incomplete lower-upper (BILU) local preconditioning of the linear system is used to ensure effectiveness of the GMRES method. The additive Schwarz preconditioning is easily implemented within the block-based anisotropic AMR scheme presented in the previous subsection. Finally, to improve the global convergence of the Newton algorithm, an implicit Euler time-marching startup procedure with switched evolution/relaxation (SER), as proposed by Mulder and Van Leer,<sup>83</sup> is also applied.

## VIII. Numerical Results for Radiation Transport in Non-Gray Gases

In this section, the predictive capabilities of the newly-developed interpolative-based non-gray second-order maximum-entropy,  $M_2$ , moment closure are assessed by comparison of its solutions to those of its lower-order counterpart, i.e., the non-gray  $M_1$  closure, as well as those of the more commonly adopted first- and third-order spherical harmonic moment closures,  $P_1$ , and  $P_3$ , respectively, and the DOM, for a range of test cases involving non-gray radiative heat transfer in real gases. In addition to the total (spectrally integrated) radiative energy density,  $I^{(0)} = \int_0^\infty I_\eta^{(0)} d\eta$ , and the total radiative heat flux,  $I^{(1)} = \int_0^\infty I_\eta^{(1)} d\eta$ , comparisons are also performed in terms of the total radiative source term,  $S_R$ , as defined in Eq. (42), which contributes to the source term in the conservation of energy equation. In all the cases studied, the spectral dependence of the radiative properties of participating (absorbing, emitting and/or scattering) gases is treated using the statistical narrow-band correlated- $k$  (SNBCK) model, and steady-state numerical solutions for the non-gray  $M_2$  closure are obtained using the Godunov-type finite volume scheme described above.

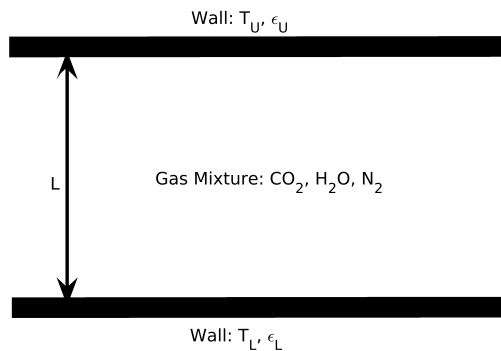


Figure 3. Illustration of parallel plate test case for non-gray radiation.

Table 3. Computational Conditions for Parallel Plate Test Cases.

| Case | L (m)       | Temperature Distribution                                  | Mixture  |
|------|-------------|---|--|
| 1    | 0.1 and 1.0 | Uniform at 1000 K   | Pure H <sub>2</sub> O  |
| 2    | 1.0         | Uniform at 1000 K   | N <sub>2</sub> and H <sub>2</sub> O with $f_{\text{H}_2\text{O}} = 4 \left(1 - \frac{x}{L}\right) \frac{x}{L}$ |
| 3    | 0.2         | $T = T_U + (T_L - T_U) \left(1 - \frac{x}{L}\right)^{10}$ | Pure H <sub>2</sub> O  |
| 4    | 0.5         | $T = T_U + (T_L - T_U) \left(1 - \frac{x}{L}\right)^{10}$ | 10% CO <sub>2</sub> , 20% H <sub>2</sub> O, and 70% N <sub>2</sub> (mole basis)                                |

For all the cases studied, the method of characteristics is used to provide boundary conditions to the systems of equations arising from the moments closures of interest in the present study. In the particular case of the M<sub>1</sub> and M<sub>2</sub> closures, new generalized Roe matrices have been developed by the authors, for multi-dimensional problems, following the Multiple Averages (MAs) methodology proposed by Rosatti and Begnudelli.<sup>86</sup> The derivation of the latter matrices is not presented herein but will be the subject of future follow-on studies.

The first set of representative test problems involves radiative heat transfer between two parallel plates with given separation distance, medium temperature distribution, and gas mixture composition, similar to those studied by Liu *et al.*<sup>7</sup> as well as Sarr and Groth.<sup>31</sup> For such test cases, exact analytical solutions of the RTE are available, and are therefore used as additional references for the comparisons, similar to the work by Sarr and Groth.<sup>31</sup>

Next, the assessment of the newly-developed non-gray M<sub>2</sub> closure is applied to multi-dimensional radiative heat transfer problems by considering non-gray radiation within a rectangular enclosure, with specified distributions of the temperature and gas mixture compositions.

For all the test problems considered, comparisons are performed on grid independent solutions for the M<sub>1</sub>, M<sub>2</sub>, P<sub>1</sub>, and P<sub>3</sub> moment closures, as well as the DOM. Such solutions are obtained by comparing predictions of each of the radiation models on a sequence of increasingly refined grids and consequently choosing the mesh size for which no significant further change in the solution is observed as the mesh is further refined.

### VIII.A. Non-Gray Radiative Heat Transfer Between Parallel Plates

The geometry for the parallel plate test problems, considered in the present study for the assessment of the proposed non-gray M<sub>2</sub> closure, is illustrated in Fig. 3. The bounding wall surfaces are assumed to be black, i.e.,  $\epsilon_L = \epsilon_U = 1$ , and the medium between the two plates is non-scattering at a uniform pressure of 1 atm. The computational parameters, specific to each of the test cases related to this geometry, are summarized in Table 3. Furthermore, for a non-scattering medium confined between two black, parallel plates, there exists an exact analytical solution to the radiative transfer equation,<sup>32</sup> Eq. (1).

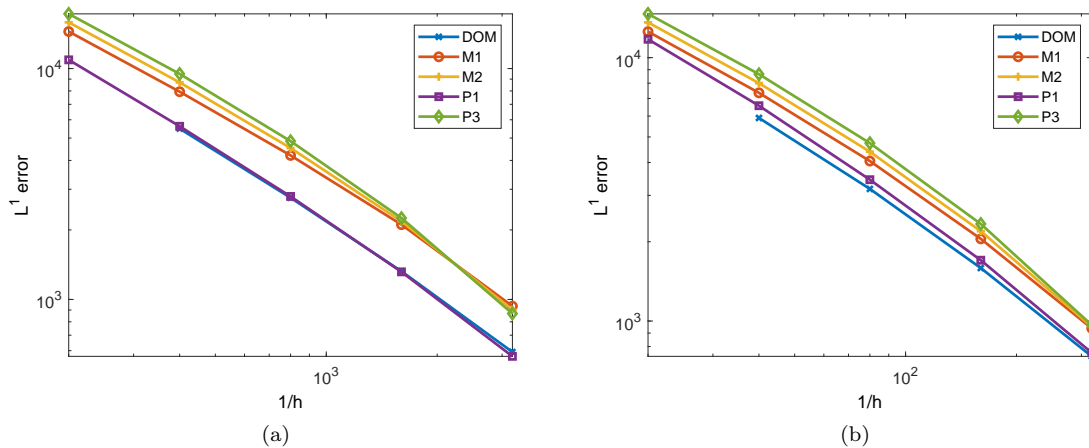


Figure 4. Illustration of grid convergence analysis on the predicted radiative source term for DOM, M<sub>1</sub>, M<sub>2</sub>, P<sub>1</sub>, and P<sub>3</sub>, for (a) the small plate separation of Case 1 ( $L = 0.1$  m), and (b) the larger plate separation of Case 1 ( $L = 1$  m).

### VIII.A.1. Parallel Plate Case 1

For the first parallel plate test problem, which is considered here to assess the ability of the proposed interpolative-based non-gray  $M_2$  closure to accurately capture radiative transfer for various optical conditions, the medium between the two plates consists of pure  $H_2O$  at a temperature of 1000 K, while the bounding walls are maintained at a cold temperature of 0 K. Two plate separation distances are considered, i.e.,  $L = 0.1$  m and  $L = 1$  m. Results of grid convergence analysis are presented in Fig. 4 for both plate separations. In addition, comparisons of the predictions of the radiative energy density, the radiative heat flux, and the radiative source term, for this test problem, are also illustrated in Figs. 5 and 6, for the small and larger plate separations, respectively. For all the radiation models considered in this study, the solutions obtained on the second-finest grid are used for the comparisons of spectrally integrated radiative quantities. This mesh resolution can be observed to fall well within the asymptotic range of convergence for both plate separations and ensures that numerical errors do not influence the comparisons of the solutions.

For the small plate separation, the  $M_1$  model provides solutions of comparable accuracy to those of the third-order spherical harmonic,  $P_3$ , moment closure, while yielding improved predictions of the radiative quantities under consideration relative to its spherical harmonic counterpart, i.e., the  $P_1$  moment closure.

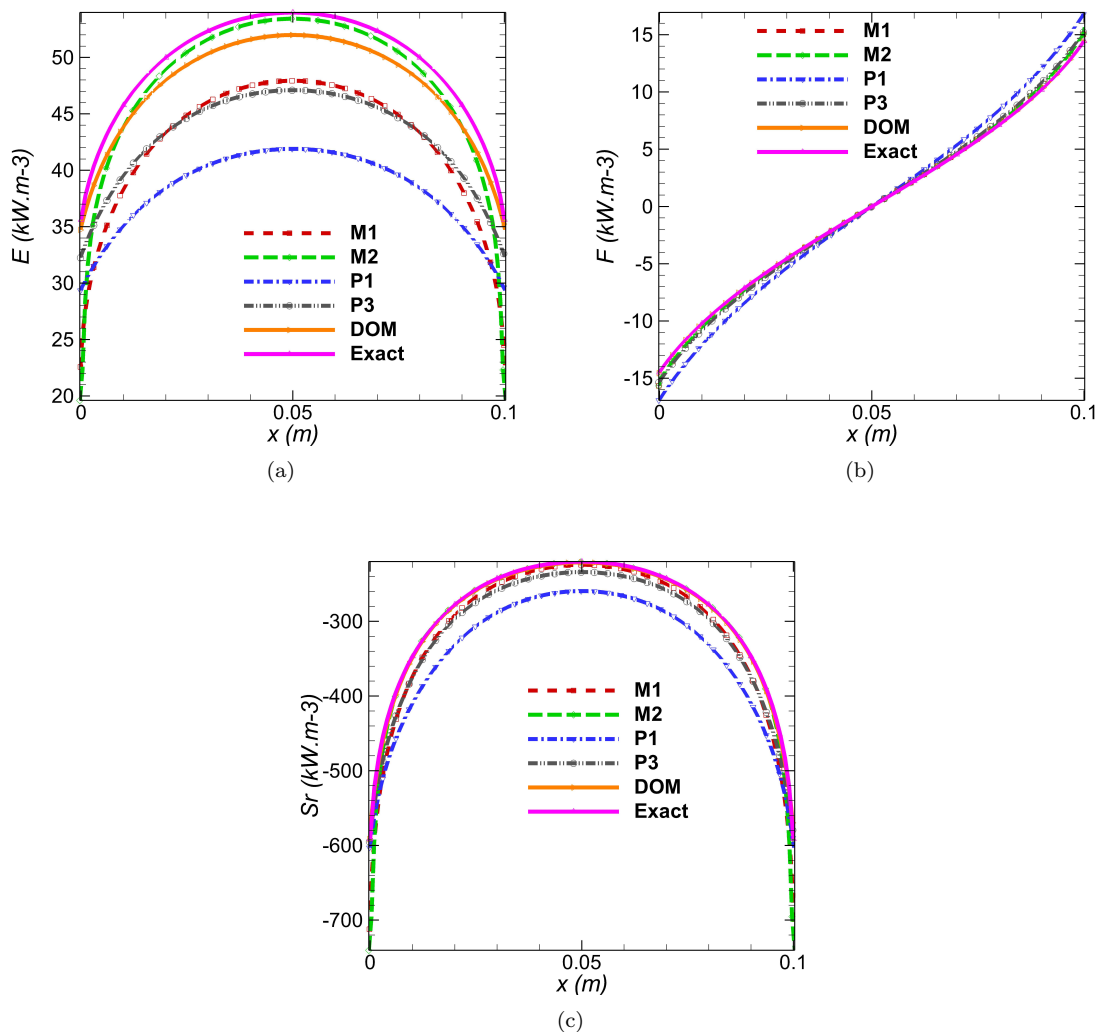
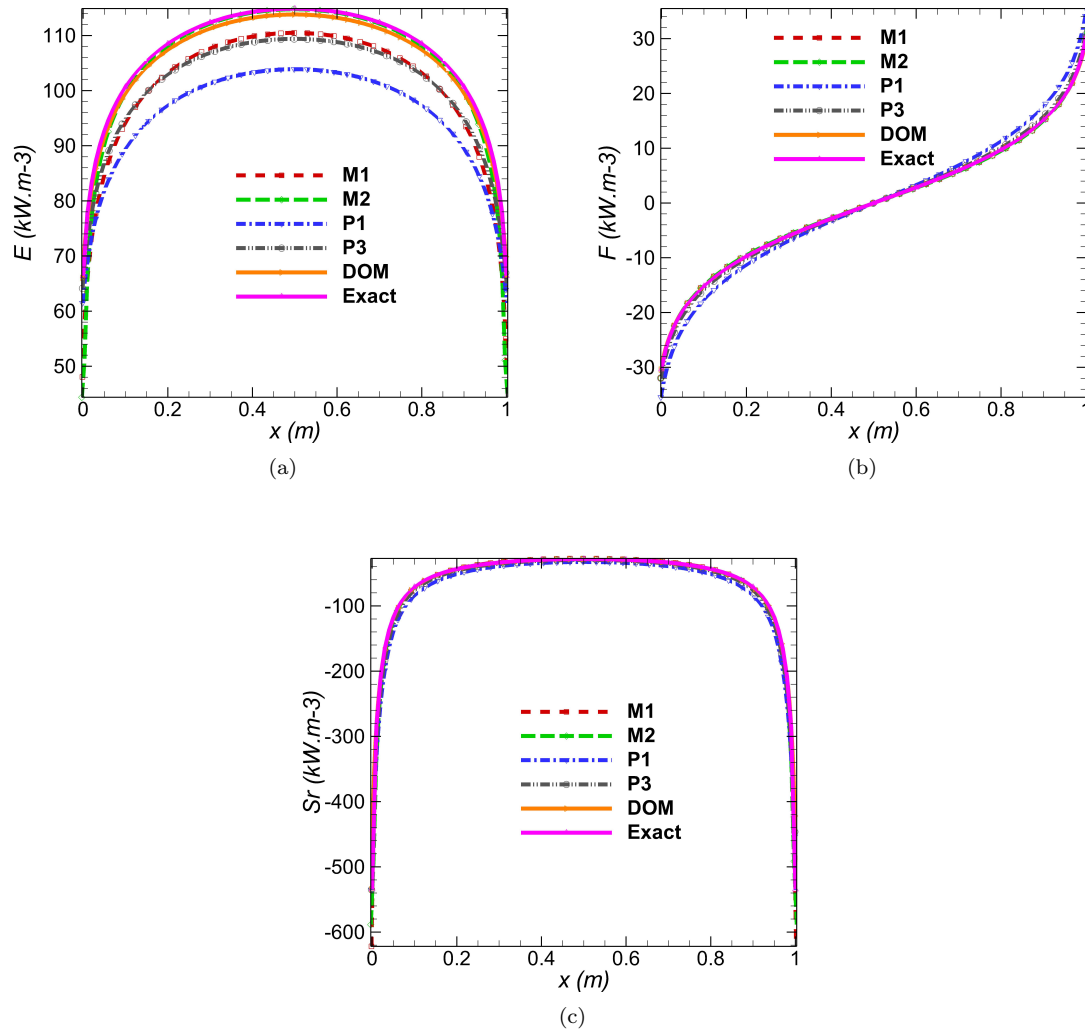


Figure 5. Predictions of (a) radiative energy density, (b) radiative heat flux, and (c) radiative source term for the small plate separation of Case 1 ( $L = 0.1$  m) obtained using the DOM, the  $M_1$ ,  $M_2$ ,  $P_1$  and  $P_3$  moment closures, with exact solution to the RTE used a reference for comparisons.



**Figure 6.** Predictions of (a) radiative energy density, (b) radiative heat flux, and (c) radiative source term for the larger plate separation of Case 1 ( $L = 1$  m) obtained using the DOM, the  $M_1$ ,  $M_2$ ,  $P_1$  and  $P_3$  moment closures, with exact solution to the RTE used as a reference for comparisons.

However, as either one of the bounding walls is approached, the radiative energy density predicted by the non-gray  $M_1$  seems to noticeably deviate from the predictions of the  $P_3$  moment closure, and provides somewhat less accurate solutions than either the  $P_1$  or  $P_3$  spherical harmonic moment closures. A similar phenomenon is also observed in the case of the radiative source term, which is directly related to the radiative energy density, as can be seen from Eq. (42). On the other hand, predictions of the radiative heat flux near the bounding walls, obtained using the  $M_1$  closure, do not display such features but are rather in good agreement with those of the  $P_3$  moment closure, as well as the DOM and the exact solution, while being superior to the predictions of the  $P_1$  closure. As can be expected, the non-gray  $M_2$  closure yields improved predictions of the radiative solutions compared to its lower-order counterpart, i.e., the non-gray  $M_1$  closure, as well as the  $P_3$  closure, and is of comparable accuracy to the DOM and the exact solutions. However, similar to the  $M_1$  closure, the distribution of the radiative energy density, as well as the radiative source term, predicted by the non-gray  $M_2$  closure also deteriorate near the bounding walls. This may point to the fact that the  $M_N$  closures cannot properly capture discontinuous temperature distributions, as is the case for the test problem under consideration.

As the plate separation is increased, similar observations as for the smaller plate separation can be made, i.e., the  $M_2$  closure again provides improved solutions compared to the  $M_1$  closure. Away from the bounding

walls, the latter closure is seen to maintain similar level of accuracy relative the the  $P_3$  moment closure, while yielding better solutions than the  $P_1$  closure. The  $M_2$  closure, on the other hand, outperforms all the other three moment closure techniques under consideration and matches both the DOM and the exact solutions. As either one of the bounding plates is approached, predictions of the radiative energy density as well as the radiative source term, for both the  $M_1$  and  $M_2$  closures, are again observed to deteriorate, compared to the  $P_1$  and  $P_3$  closures, due to the discontinuous temperature distributions near the walls.

Solutions of the radiative energy density, the radiative heat flux, as well as the radiative source term, between the two plates, obtained using the  $M_1$ ,  $M_2$ ,  $P_1$  and  $P_3$  moment closures, as well as the DOM, can be seen to be in better agreement with the exact solution for the larger plate separation, when compared to the small separation distance. In fact, as the distance between the two plates is increased, the optical thickness of radiatively absorbing and emitting media of the type considered herein (for Case 1) increases, thereby resulting in more substantial emission of radiation throughout the domain. This in turn results in distributions of radiation lying closer to the isotropic limit, as compared to smaller plate separations, characterized by smaller optical depths.

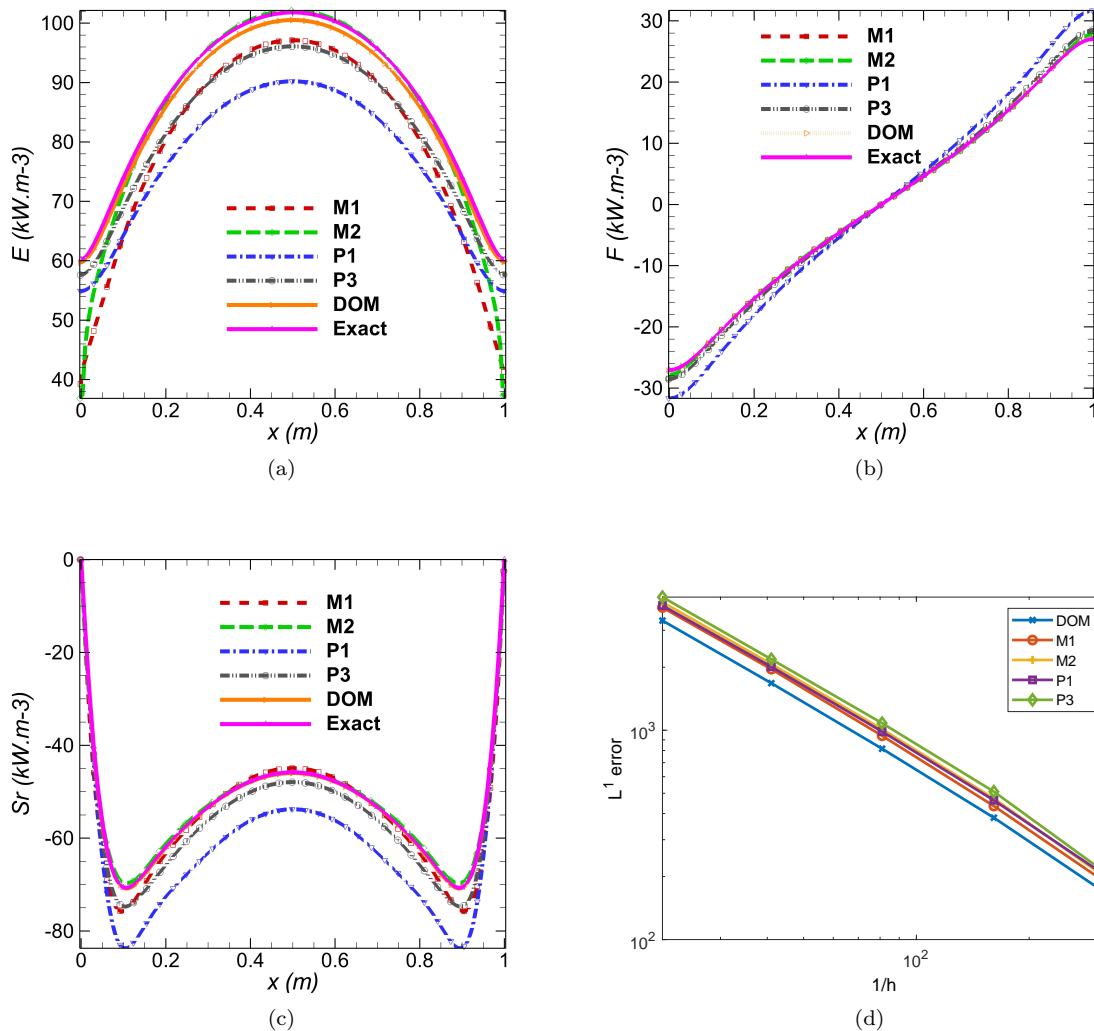


Figure 7. Predictions of (a) radiative energy density, (b) radiative heat flux, and (c) radiative source term for Case 2 ( $L = 1$  m) obtained using the DOM, the  $M_1$ ,  $M_2$ ,  $P_1$  and  $P_3$  moment closures, with exact solution to the RTE used as reference for comparisons, and (d) illustration of grid convergence analysis on the predicted radiative source term.

### VIII.A.2. Parallel Plate Case 2

The next parallel plate problem has been considered to assess the predictive capabilities of our non-gray  $M_2$  closure in the case of radiative transfer in non-homogeneous media, in particular media with spatially varying species concentrations. More specifically, for this test problem, the medium between the two plates, with separation distance  $L = 1$  m, is now a mixture of  $N_2$  and  $H_2O$ , and the distribution of the mole fraction of  $H_2O$  in the mixture is given by

$$f_{H_2O} = 4 \left(1 - \frac{x}{L}\right) \frac{x}{L}, \quad (56)$$

where  $x$  represents the distance from the lower plate and  $L = 1$  m is the separation distance between the two plates. The gas mixture is at a temperature of 1000 K, while the bounding walls are again assumed to be cold at 0 K. Similar to Case 1, a grid convergence analysis has again been performed, the results of which, for this test problem, are illustrated in Fig. 7(d). It can be seen that the solutions corresponding to the second-finest mesh, for all five of the radiation models, are indeed grid independent and are therefore used for the comparisons of total radiative quantities of interest, which are illustrated in Fig. 7.

A phenomenon similar to the one observed in Case 1, where the same temperature distribution was adopted, can be depicted in the predictions of the radiative energy density obtained using both the  $M_1$  and  $M_2$  closures. More specifically, the solutions provided by the latter closures, in terms of the radiative energy density, are again observed to deteriorate as either one of the walls is approached. Unlike Case 1 however, the same phenomenon is not observed for the total radiative source term, which is due to the distribution of the concentration of radiatively participating gases. In fact, the mole fraction of water vapour,  $H_2O$ , which is the only absorbing/emitting specie in the gas mixture considered in this test problem ( $N_2$  is an inert gas), vanishes as either wall is approached. This explains the fact that the radiative source term predicted by all of the approximate radiation models considered in the present study, in addition to the exact solution, vanishes, due to its direct proportionality to the absorption coefficient. To the exception of the latter phenomena, the solutions provided by the  $M_1$  closure are of comparable accuracy to those of the  $P_3$  closure and superior to the predictions of the  $P_1$  closure. The  $M_2$  closure on the other hand yields improved predictions of the radiative quantities, relative to the  $M_1$  closure, as can again be expected, and matches both the DOM and the exact solutions, while outperforming the  $P_N$  closures considered in this study.

### VIII.A.3. Parallel Plate Case 3

In addition to spatially varying species concentrations, location-dependent temperature distributions are also commonly encountered in practical applications, and are considered in the present assessment of the proposed non-gray  $M_2$  closure, for the sake of completeness. Thus parallel plate Case 3 is examined next, which involves radiative transfer between two parallel plates with a separation distance  $L = 0.2$  m. The medium between the plates consists of pure  $H_2O$ , with a temperature distribution of the form

$$T = T_U + (T_L - T_U) \left(1 - \frac{x}{L}\right)^{10}, \quad (57)$$

where again  $x$  represents the distance from the lower plate, and  $T_U = 300$  K and  $T_L = 1500$  K represent the temperature on the upper and lower walls, respectively. Similar to the previous test cases, i.e., Case 1 and 2, grid convergence studies are performed on the solutions of the DOM,  $M_1$ ,  $M_2$ ,  $P_1$  and  $P_3$  radiation models, in particular on the predicted total radiative source term, as can be depicted in Fig. 8(d). Moreover, numerical predictions of total radiative energy density, total radiative heat flux, and total radiative source term for Case 3 are also illustrated in Fig. 8.

The results shown in the latter figure were again obtained on the second finest mesh, which, as can be seen in Fig. 8(d), corresponds to grid-converged solutions well within the asymptotic range of convergence. The numerical results show that the  $M_1$  closure substantially underpredicts the radiative energy density and is less accurate than both the  $P_1$  and  $P_3$  closures, as far as the latter radiative quantity is concerned. On the other hand, solutions of the radiative heat flux obtained using the  $M_1$  closure are superior to those of the  $P_1$  closure, though still not as accurate as the  $P_3$  closure. In terms of the radiative source term, the  $M_1$  closure can be seen to be at least as accurate as the  $P_3$  spherical harmonic moment closure, as far as the DOM and the exact solutions are concerned, and is again superior to the  $P_1$  closure, especially in the region where the peak occurs. Improvements in the predictions of the radiative quantities, relative to the  $M_1$  closure, can be achieved, as can be expected, by considering higher-order members of the hierarchy of  $M_N$

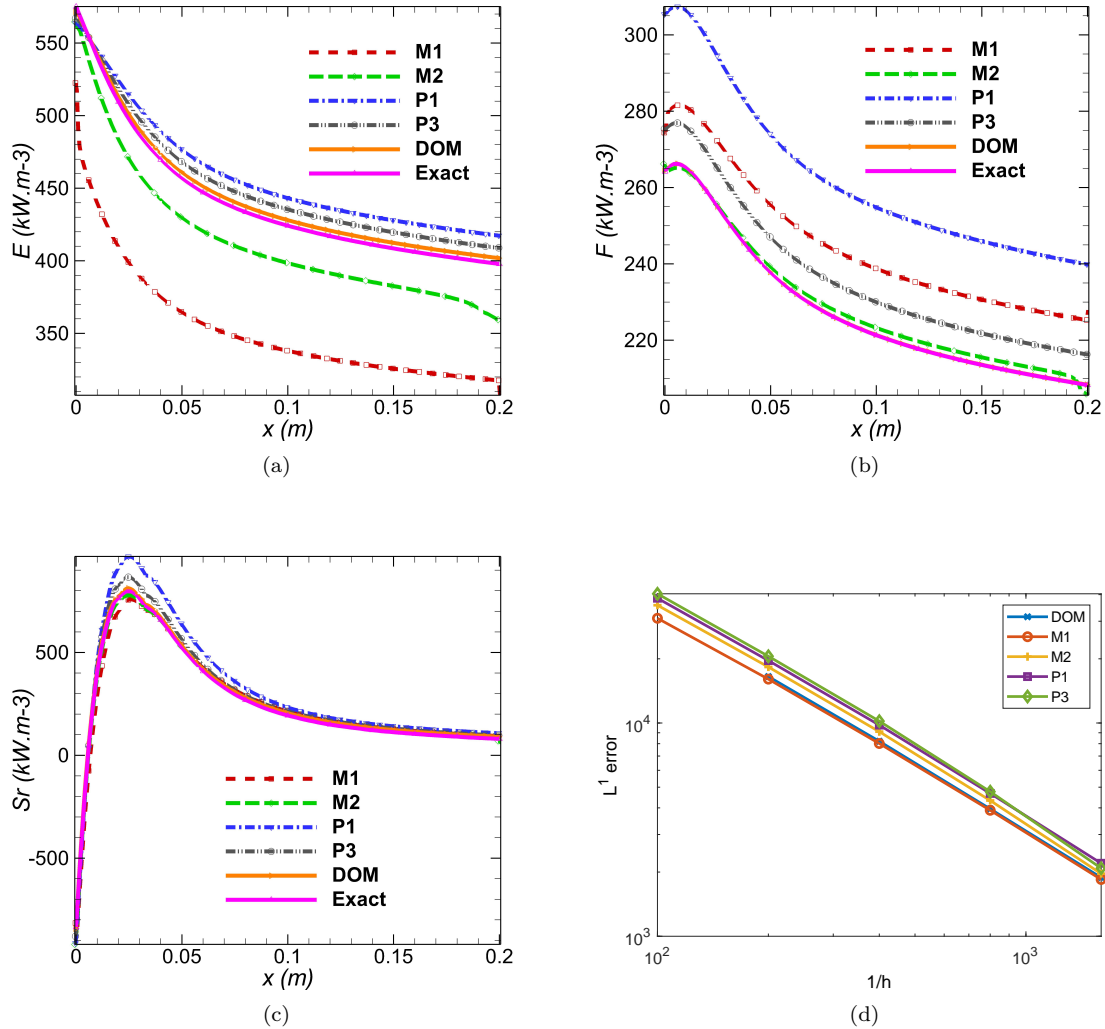


Figure 8. Predictions of (a) radiative energy density, (b) radiative heat flux, and (c) radiative source term for Case 3 ( $L = 0.2$  m) obtained using the DOM, the  $M_1$ ,  $M_2$ ,  $P_1$  and  $P_3$  moment closures, with exact solution to the RTE used as reference for comparisons, and (d) illustration of grid convergence analysis on the predicted radiative source term.

closures, in particular the  $M_2$  closure. The latter closure is observed to provide substantial improvements in the solutions of the radiative energy density, relative to its lower-order counterpart, though still not as accurate as the  $P_N$  closures studied herein. However, for both the radiative heat flux and the radiative source term, the solutions of the  $M_2$  closure outperform, once again, the  $M_1$ ,  $P_1$ , and  $P_3$  moment closures and are of comparable accuracy to those of both the exact solutions and the DOM.

#### VIII.A.4. Parallel Plate Case 4

Similar to Case 3, the last test problem involving radiative transfer between parallel plates seeks to assess the predictive capabilities of our non-gray  $M_2$  closure for non-gray radiative transfer in non-isothermal media. Unlike Case 3 however, the present test problem involves a radiatively participating gas mixture consisting of 10%  $\text{CO}_2$ , 20%  $\text{H}_2\text{O}$ , and 70%  $\text{N}_2$ , where the percentages are given on a mole basis, and the plate separation is  $L = 0.5$  m. Results of grid convergence analysis, based on the predicted radiative source term, for all the approximate radiation models of interest in the present study, are presented in Fig. 9(d). Furthermore, numerical predictions of total radiative energy density, total radiative heat flux, and total radiative source term, obtained on the second-finest mesh, are illustrated in Fig. 9.

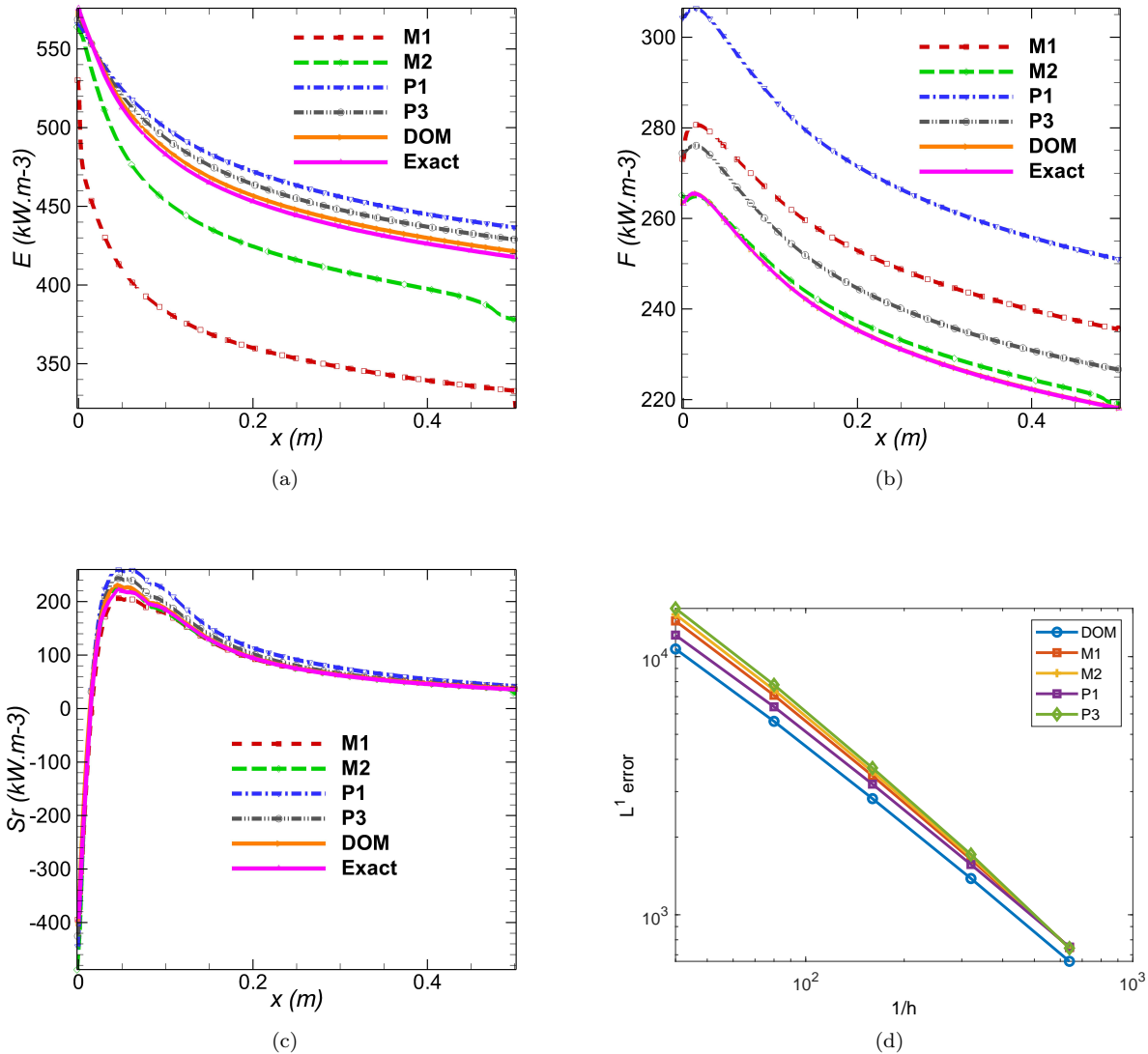


Figure 9. Predictions of (a) radiative energy density, (b) radiative heat flux, and (c) radiative source term for Case 4 ( $L = 0.5$  m) obtained using the DOM, the  $M_1$ ,  $M_2$ ,  $P_1$  and  $P_3$  moment closures, with exact solution to the RTE used as reference for comparisons, and (d) illustration of grid convergence analysis on the predicted radiative source term.

The numerical results associated with this test problem show similar trends to those obtained for Case 3, which is expected since the only differences between the two cases, i.e., Case 3 and Case 4, are the composition of the radiatively participating gas mixture and the separation distance between the two plates. In particular, the  $P_1$  and  $P_3$  closures provide more accurate predictions of the radiative energy density compared to the non-gray  $M_2$  closure, which yields improved predictions compared to the  $M_1$  closure for which substantial underestimations of the energy density are observed. As far as the radiative heat flux and the radiative source term, the  $P_1$  and  $P_3$  closures are outperformed by the  $M_2$  closure which displays similar levels of accuracy as the DOM and the exact solutions. It should also be noted that, in the case of the radiative source term, even the  $M_1$  closure is at least as accurate as the  $P_3$  closure and is superior to the  $P_1$  closure, especially in the region where the peak values are observed.

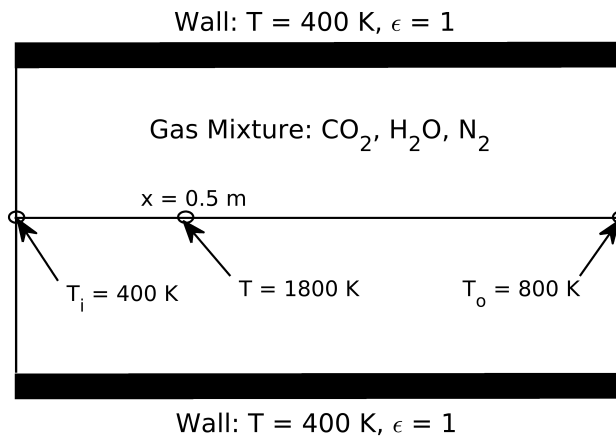


Figure 10. Illustration of rectangular enclosure test case for non-gray radiation.

### VIII.B. Non-Gray Radiative Heat Transfer within Rectangular Enclosures

Radiative heat transfer within a rectangular enclosure is now considered. The geometry of the latter, which is 4 m long and has a width of 2 m, is illustrated in Fig. 10. The surrounding walls are black and cold at 400 K, while the gas mixture within the enclosure, which consists of 20% H<sub>2</sub>O, 10% CO<sub>2</sub>, and 70% N<sub>2</sub>, where the percentages are expressed on a mole basis, is maintained at atmospheric pressure. The temperature of the gas inside the enclosure is not uniform but instead follows a distribution that is symmetric with respect to the centreline of the enclosure, and has the following form:

$$T = T_w + (T_c - T_w) (1 - 3|y|^2 + 2|y|^3), \quad (58)$$

where  $y$  corresponds to the radial distance from the centreline,  $T_w = 400$  K represents the walls temperature, and  $T_c$  is the centreline temperature. The latter is assumed to increase quadratically from  $T_i = 400$  K at the inlet ( $x = 0$  m) to 1800 K at  $x = 0.5$  m, then decreases quadratically to  $T_o = 800$  K at the exit ( $x = 4$

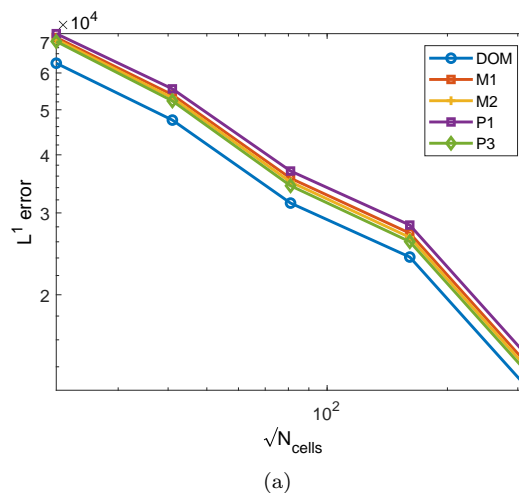


Figure 11. Illustration of grid convergence analysis on the predicted radiative source term for DOM, M<sub>1</sub>, M<sub>2</sub>, P<sub>1</sub>, and P<sub>3</sub>, for Case 5, involving radiative heat transfer in a rectangular enclosure.

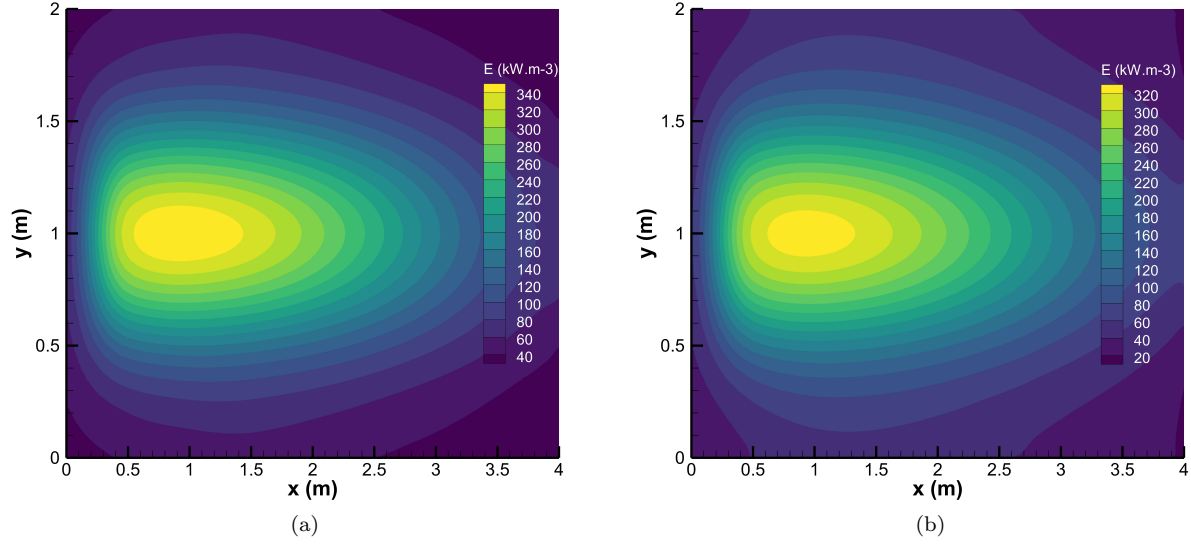


Figure 12. Contours of radiative energy density predicted by (a) the DOM, and (b) the non-gray  $M_2$  closure for the rectangular enclosure test problem.

m) via the following distribution

$$T_c = \begin{cases} -5600x^2 + 5600x + 400, & x < 0.5, \\ -\frac{1000}{12.25}x^2 + \frac{1000}{12.25}x + \frac{21800}{12.25}, & x \geq 0.5. \end{cases} \quad (59)$$

Results of grid convergence analysis on the total radiative source term, for the DOM, as well as the  $M_1$ ,  $M_2$ ,  $P_1$ , and  $P_3$  moment closure techniques, are illustrated in Fig. 11. Moreover, predicted contours of total radiative energy density,  $I^{(0)}$ , within the rectangular enclosure are shown in Figs. 12(a) and (b) for the DOM and our non-gray  $M_2$  closure, respectively. As can be expected, the radiative energy density takes its maximum values near the location of maximum temperature along the centreline, and then decreases towards either the inlet or the outlet, or radially towards the relatively cold walls, and such a behaviour is well captured by both the DOM and our non-gray  $M_2$  closure.

Numerical predictions of the total radiative energy density, total radiative heat flux, and total radiative source term, along the centreline of the rectangular enclosure, obtained using our non-gray  $M_2$  closure, are now compared to those of the  $M_1$ ,  $P_1$  and  $P_3$  moment closures, as well as those of the DOM, as shown in Fig. 13. It is worth mentioning that, due to the lack of exact analytical solutions to the equation of radiative transfer for this particular problem, solutions of the DOM are used as benchmark for the comparisons. The numerical results presented here show that even the non-gray  $M_1$  closure provides solutions of the radiative energy density and the radiative source term as least as accurate as to those of the  $P_3$  moment closure, while being superior to the predictions of the  $P_1$  moment closure technique. Furthermore, the non-gray  $M_2$  closure yields improved predictions of the radiation solutions compared to its lower-order counterpart and is in better agreement with the DOM, when compared to the  $M_1$ ,  $P_1$ , and  $P_3$  radiation models.

## IX. Conclusions

Inspired by the many desirable properties of maximum entropy closures, a new, computationally efficient interpolative-based approximation of the second-order maximum-entropy,  $M_2$ , moment closure for predicting radiative heat transfer in non-gray participating media has been developed, thoroughly described, and applied to a number of representative problems to investigate its predictive capabilities. By construction, the present closure accurately mimics maximum entropy solutions for the third-order closing fluxes for all physically realizable moments sets up to second order over the full spectrum of frequencies and also appears to be globally hyperbolic. The latter was shown numerically but not proven. After describing the implementation

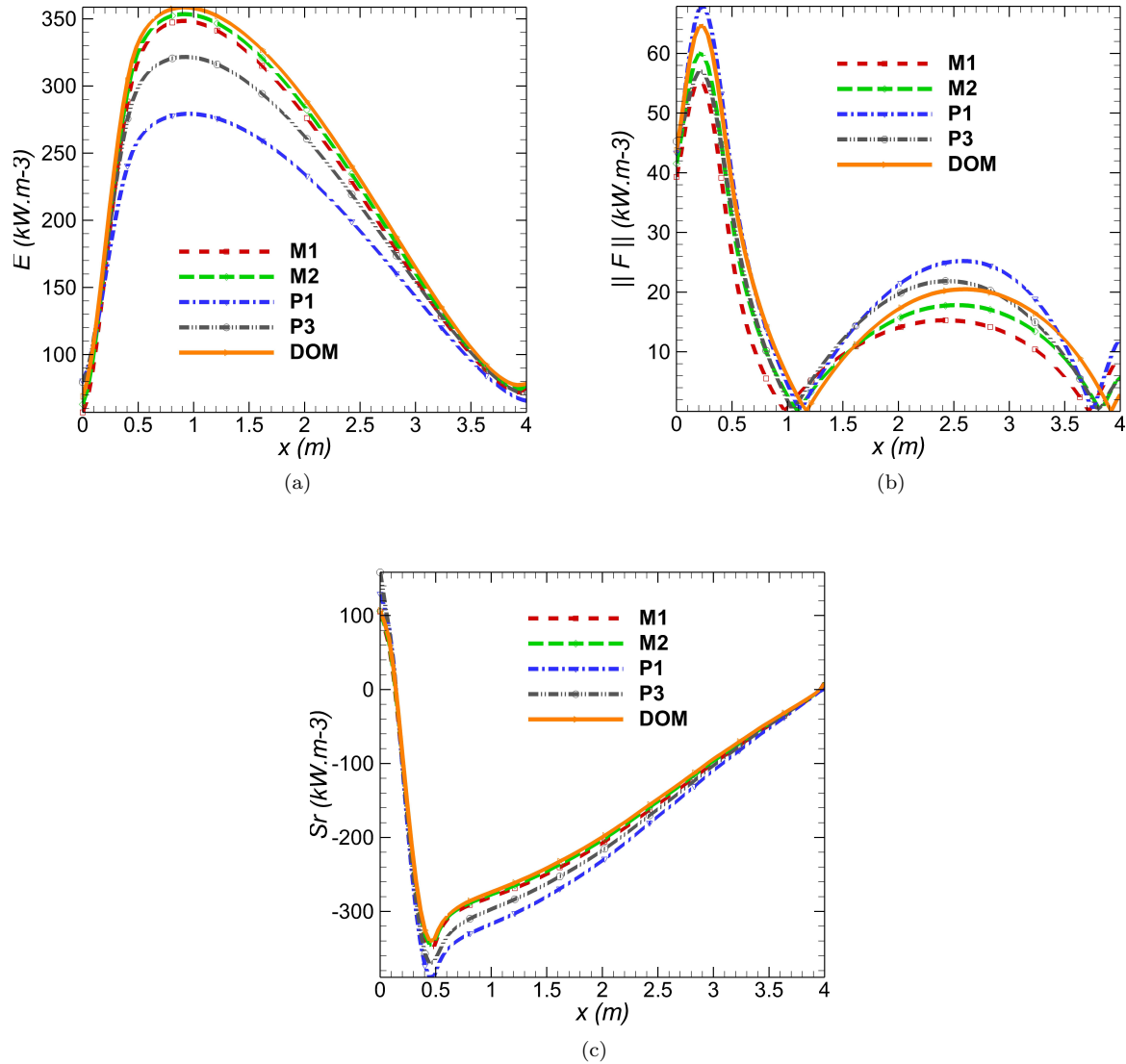


Figure 13. Predictions of (a) radiative energy density, (b) radiative heat flux, and (c) radiative source term for the rectangular enclosure test case obtained using the DOM, the  $M_1$ ,  $M_2$ ,  $P_1$  and  $P_3$  moment closures, with the DOM used as a benchmark for comparisons.

of our non-gray  $M_2$  closure in the context of existing state-of-the-art spectral radiation models, in particular the statistical narrow-band correlated- $k$  technique, its ability to predict radiative heat transfer in non-gray participating media for various one- and two-dimensional canonical problems has been assessed by comparing predicted solutions to those of other approximate radiation solution techniques, including the  $M_1$ ,  $P_1$ , and  $P_3$  moment closures, as well as the DOM. For virtually all the test problems considered, the solutions of the proposed non-gray  $M_2$  closure were observed to be largely superior to those of either lower-order moment closure (i.e., the  $M_1$  and  $P_1$  models). Furthermore, for almost all cases, the non-gray  $M_2$  closure was superior to the  $P_3$  spherical harmonic moment closure, while achieving similar levels of accuracy compared to the standard discrete ordinates method, as far as numerical predictions of the radiative energy density, the radiative heat flux, and the radiative source term are concerned.

Future research will involve the extension of the assessment of our interpolative-based non-gray  $M_2$  closure to both laminar and turbulent reactive flows with soot formation. Reynolds-averaged Navier-Stokes (RANS)-based turbulent simulations will be considered, whereby suitable modelling of the turbulence-radiation inter-

actions, arising from the highly nonlinear closure relations for the non-gray second-order maximum-entropy,  $M_2$ , moment closure, will be proposed. Implementation of the non-gray  $M_2$  closure will also be considered in the context of the full spectrum correlated- $k$  (FSCK) spectral radiation model. The FSCK is in fact expected to provide more efficient approximate radiation solutions, relative to the SNBCK model, as the reordering procedure for the spectral absorption coefficient is applied to the full spectrum of frequencies, such that the total number of quadrature points required for integration over the full range of wavenumbers is reduced, compared to the SNBCK treatment.

## Acknowledgments

This research was funded by grants and contracts from the Green Aviation Research and Development Network (GARDN), Southern Ontario Smart Computing for Innovation Platform (SOSCIP), as well as Pratt & Whitney Canada. The first author also received support in the form of a scholarship from the Natural Sciences and Engineering Research Council (NSERC) of Canada as well as the Ontario Graduate Scholarship (OGS) from the province of Ontario and the university of Toronto. Additionally, the computational resources for performing the numerical simulations reported herein were provided by the SOSCIP program as well as the SciNet High Performance Computing Consortium at the University of Toronto and Compute/Calcul Canada (the latter are funded by the Canada Foundation for Innovation (CFI) and Province of Ontario, Canada).

## References

- <sup>1</sup>Sachdev, J. S., Groth, C. P. T., and Gottlieb, J. J., "A Parallel Solution-Adaptive Scheme for Predicting Multi-Phase Core Flows in Solid Propellant Rocket Motors," *International Journal of Computational Fluid Dynamics*, Vol. 19, No. 2, 2005, pp. 159–177.
- <sup>2</sup>Gao, X. and Groth, C. P. T., "A Parallel Adaptive Mesh Refinement Algorithm for Predicting Turbulent Non-Premixed Combusting Flows," *International Journal of Computational Fluid Dynamics*, Vol. 20, No. 5, 2006, pp. 349–357.
- <sup>3</sup>Groth, C. P. T. and McDonald, J. G., "Towards Physically-Realizable and Hyperbolic Moment Closures for Kinetic Theory," *Continuum Mechanics and Thermodynamics*, Vol. 21, No. 6, 2009, pp. 467–493.
- <sup>4</sup>Gao, X., Northrup, S. A., and Groth, C. P. T., "Parallel Solution-Adaptive Method for Two-Dimensional Non-Premixed Combusting Flows," *Progress in Computational Fluid Dynamics*, Vol. 11, No. 2, 2011, pp. 76–95.
- <sup>5</sup>Charest, M. R. J., Groth, C. P. T., and Gülder, Ö. L., "Solution of the Equation of Radiative Transfer Using a Newton-Krylov Approach and Adaptive Mesh Refinement," *Journal of Computational Physics*, Vol. 231, 2012, pp. 3023–3040.
- <sup>6</sup>McDonald, J. G., Sachdev, J. S., and Groth, C. P. T., "Application of Gaussian Moment Closure to Micro-Scale Flows with Moving and Embedded Boundaries," *AIAA Journal*, Vol. 51, No. 9, 2014, pp. 1839–1857.
- <sup>7</sup>Liu, F., Smallwood, G. J., and Gülder, Ö. L., "Application of the Statistical Narrow-Band Correlated- $k$  Method to Low-Resolution Spectral Intensity and Radiative Heat Transfer Calculations — Effects of the Quadrature Scheme," *International Journal of Heat and Mass Transfer*, Vol. 43, No. 17, 2000, pp. 3119–3135.
- <sup>8</sup>Liu, F., Smallwood, G. J., and Gülder, Ö. L., "Band Lumping Strategy for Radiation Heat Transfer Calculations using a Narrowband Model," *Journal of Thermophysics and Heat Transfer*, Vol. 14, No. 2, 2000, pp. 278–281.
- <sup>9</sup>Liu, F., Smallwood, G. J., and Gülder, Ö. L., "Application of the Statistical Narrow-Band Correlated- $k$  Method to Non-Grey Gas Radiation in CO<sub>2</sub>-H<sub>2</sub>O Mixtures: Approximate Treatments of Overlapping Bands," *Journal of Quantitative Spectroscopy and Radiative Transfer*, Vol. 68, No. 4, 2001, pp. 401–417.
- <sup>10</sup>Modest, M. F. and Zhang, H., "The Full-Spectrum Correlated- $k$  Distribution for Thermal Radiation From Molecular Gas-Particulate Mixtures," *Journal of Heat Transfer*, Vol. 124, 2002, pp. 30.
- <sup>11</sup>W. A. Fiveland, W. A., "Discrete-Ordinates Solutions of the Radiative Transport Equation for Rectangular Enclosures," *Journal of Heat Transfer*, Vol. 106, No. 4, 1984, pp. 699–706.
- <sup>12</sup>Grad, H., "On the Kinetic Theory of Rarefied Gases," *Communications on Pure and Applied Mathematics*, Vol. 2, 1949, pp. 331–407.
- <sup>13</sup>Mazumder, S. and Modest, M. F., "A Probability Density Function Approach to Modeling Turbulence-Radiation Interactions in Nonluminous Flames," *International Journal of Heat and Mass Transfer*, Vol. 42, No. 6, 1999, pp. 971–991.
- <sup>14</sup>Modest, M. F. and Mehta, R. S., "Modeling Absorption TRI in Optically Thick Eddies," *Proceedings of Eurotherm78 - Computational Thermal Radiation in Participating Media II*, Vol. 78, 2006, pp. 225–234.
- <sup>15</sup>Li, G. and Modest, M. F., "Importance of Turbulence-Radiation Interactions in Turbulent Diffusion Jet Flames," *Journal of Heat Transfer*, Vol. 125, No. 5, 2003, pp. 831–838.
- <sup>16</sup>Gupta, A., Modest, M. F., and Haworth, D. C., "Large-Eddy Simulation of Turbulence-Radiation Interactions in a Turbulent Planar Channel Flow," *Journal of Heat Transfer*, Vol. 131, No. 6, 2009, pp. 061704–1–061704–8.
- <sup>17</sup>Dubroca, B. and Feugeas, J.-L., "Theoretical and Numerical Study on a Moment Closure Hierarchy for the Radiative Transfer Equation," *SIAM Journal on Numerical Analysis*, Vol. 329, 1999, pp. 915–920.
- <sup>18</sup>Jaynes, E. T., "Information Theory and Statistical Mechanics," *Physical Review*, Vol. 106, 1957, pp. 620–630.
- <sup>19</sup>Hauck, C. D., "High-Order Entropy-Based Closures for Linear Transport in Slab Geometry," Report ORNL/TM-6023, Oak Ridge National Laboratory, 2010.

- <sup>20</sup>Hauck, C. D., “High-Order Entropy-Based closures for Linear Transport in Slab Geometry,” *Communications in Mathematical Sciences*, Vol. 9, No. 1, 2011, pp. 187–205.
- <sup>21</sup>Brunner, T. A. and Holloway, J. P., “One-Dimensional Riemann Solvers and the Maximum Entropy Closure,” *Journal of Quantitative Spectroscopy and Radiative Transfer*, Vol. 69, 2001, pp. 543–566.
- <sup>22</sup>Monreal, P. and Frank, M., “Higher Order Minimum Entropy Approximations in Radiative Transfer,” arXiv Online Article arXiv:0812.3063v1, Cornell University Library, 2008.
- <sup>23</sup>Pichard, T., Alldredge, G. W., Brull, S., Dubroca, B., and Frank, M., “An Approximation of the M<sub>2</sub> Closure: Application to Radiotherapy Dose Simulation,” *Journal of Scientific Computing*, Vol. 71, No. 1, 2017, pp. 71–108.
- <sup>24</sup>Sarr, J. A. R. and Groth, C. P. T., “Maximum-Entropy Inspired Interpolative Closure for Radiative Heat Transfer in Gray Participating Media,” *Proceedings of the 9th International Symposium on Radiative Transfer, RAD-19, June 3-7, 2019, Athens, Greece*, International Centre for Heat and Mass Transfer, 2019, pp. 253–260.
- <sup>25</sup>Sarr, J. A. R. and Groth, C. P. T., “A second-order maximum-entropy inspired interpolative closure for radiative heat transfer in gray participating media,” *Journal of Quantitative Spectroscopy and Radiative Transfer*, Vol. 255, 2020, pp. 107–238.
- <sup>26</sup>Li, R. and Li, W., “3D B<sub>2</sub> Model for Radiative Transfer Equation Part I: Modelling,” *International Journal of Numerical Analysis and Modeling*, Vol. 17, No. 1, 2020, pp. 118–150.
- <sup>27</sup>Turpault, R., “Construction of a Multigroup M1 Model for the Radiative Transfer Equations,” *C. R. Acad. Sci. Paris*, Vol. Ser. I 334, 2002, pp. 331–336.
- <sup>28</sup>Turpault, R., “A Consistent Multigroup Model for Radiative Transfer and its Underlying Mean Opacities,” *Journal of Quantitative Spectroscopy and Radiative Transfer*, Vol. 94, 2005, pp. 357–371.
- <sup>29</sup>Taine, J. and Soufiani, A., “Gas IR Radiative Properties: From Spectroscopic Data to Approximate Models,” *Advances in Heat Transfer*, Vol. 33, 1999, pp. 295–414.
- <sup>30</sup>Sarr, J. A. R., Groth, C. P. T., and Hu, J. T. C., “A Maximum Entropy-Inspired Interpolative Closure for the Prediction of Radiative Heat Transfer in Laminar Co-Flow Diffusion Flames,” *Combustion Science and Technology*, Vol. doi.org/10.1080/00102202.2019.1678376, 2019, pp. 1–35.
- <sup>31</sup>Sarr, J. A. R. and Groth, C. P. T., “A first-order maximum-entropy-inspired interpolative closure for radiative heat transfer in non-gray participating media,” *Journal of Quantitative Spectroscopy and Radiative Transfer*, 2022.
- <sup>32</sup>Modest, M. F., *Radiative Heat Transfer*, Academic Press, New York, 3rd ed., 2013.
- <sup>33</sup>Lathrop, K. D. and Carlson, B. G., “Discrete Ordinates Angular Quadrature of the Neutron Transport Equation,” Report LA 3186, Los Alamos Scientific Laboratory, 1965.
- <sup>34</sup>Thurgood, C. P., Pollard, A., and Becker, H. A., “The T<sub>N</sub> Quadrature Set for the Discrete Ordinates Method,” *ASME Journal of Heat Transfer*, Vol. 117, No. 4, 1995, pp. 1068–1070.
- <sup>35</sup>Coelho, P. J., “The Role of Ray Effects and False Scattering on the Accuracy of the Standard and Modified Discrete Ordinates Methods,” *Journal of Quantitative Spectroscopy and Radiative Transfer*, Vol. 73, No. 2-5, 2002, pp. 231–238.
- <sup>36</sup>Coelho, P. J., “Bounded Skew High-Order Resolution Schemes for the Discrete Ordinates Method,” *Journal of Computational Physics*, Vol. 175, No. 2, 2002, pp. 412–437.
- <sup>37</sup>Sakami, M., El Kasmī, A., and Charette, A., “Analysis of Radiative Heat Transfer in Complex Two-Dimensional Enclosures With Obstacles Using the Modified Discrete Ordinates Method,” *Journal of Heat Transfer*, Vol. 123, No. 5, 2001, pp. 892–900.
- <sup>38</sup>Koch, R., Krebs, W., Wittig, S., and Viskanta, R., “Discrete Ordinates Quadrature Schemes for Multidimensional Radiative Transfer,” *Journal of Quantitative Spectroscopy and Radiative Transfer*, Vol. 53, No. 4, 1995, pp. 353–372.
- <sup>39</sup>Ramankutty, M. A. and Crosbie, A. L., “Modified Discrete Ordinates Solution of Radiative Transfer in Two-Dimensional Rectangular Enclosures,” *Journal of Quantitative Spectroscopy and Radiative Transfer*, Vol. 57, No. 1, 1997, pp. 107–140.
- <sup>40</sup>Amiri, H., Mansouri, S. H., and Coelho, P. J., “Application of the modified Discrete Ordinates Method with the Concept of Blocked-Off Region to Irregular Geometries,” *International Journal of Thermal Sciences*, Vol. 50, No. 4, 2011, pp. 515–524.
- <sup>41</sup>Modest, M. F., *Radiative Heat Transfer*, Academic Press, New York, 2nd ed., 2003.
- <sup>42</sup>Jean, J. H., “The Equations of Radiative Transfer of Energy,” *Monthly Notices of the Royal Astronomical Society*, Vol. 78, No. 1, 1917, pp. 28–36.
- <sup>43</sup>Menguc, M. P. and Viskanta, R., “Radiative Transfer in Three-Dimensional Rectangular Enclosures Containing Inhomogeneous Anisotropically Scattering Media,” *Journal of Quantitative Spectroscopy and Radiative Transfer*, Vol. 33, 1985, pp. 533–549.
- <sup>44</sup>Marshak, R. E., “Note on the Spherical Harmonic Method As Applied to the Milne Problem for a Sphere,” *Physical Review*, Vol. 71, No. 7, 1947, pp. 443–446.
- <sup>45</sup>Arpaci, V. S. and Gözü̇m, D., “Thermal stability of Radiating Fluids: The Bénard Problem,” *Physics of Fluids*, Vol. 16, No. 5, 1973, pp. 581–588.
- <sup>46</sup>Fort, J., “Information-theoretical approach to radiative transfer,” *Physica A: Statistical Mechanics and its Applications*, Vol. 243, No. 3-4, 1997, pp. 275–303.
- <sup>47</sup>Johnson, S. G., “The NLOpt Nonlinear-Optimization Package,” <http://github.com/stevengj/nlopt>, 2014.
- <sup>48</sup>Kraft, D., “A Software Package for Sequential Quadratic Programming,” Technical Report DFVLR-FB 88-28, Institut für Dynamik der Flugsysteme, Oberpfaffenhofen, July 1988.
- <sup>49</sup>Kraft, D., “Algorithm 733; TOMP—Fortran Modules for Optimal Control Calculations,” *ACM Transactions on Mathematical Software*, Vol. 20, No. 3, 1994, pp. 262–281.
- <sup>50</sup>Alldredge, G. W., Hauck, C. D., O’Leary, D. P., and Tits, A. L., “Adaptive Change of Basis in Entropy-Based Moment Closures for Linear Kinetic Equations,” *Journal of Computational Physics*, Vol. 258, 2014, pp. 489–508.
- <sup>51</sup>Alldredge, G. W., Hauck, C. D., and Tits, A. L., “High-Order Entropy-Based Closures for Linear Transport in Slab Geometry II: A Computational Study of the Optimization Problem,” *SIAM Journal on Scientific Computing*, Vol. 34, No. 4, 2012, pp. B361–B391.

- <sup>52</sup>Abramov, R. V., “An Improved Algorithm for the Multidimensional Moment-Constrained Maximum Entropy Problem,” *Journal of Computational Physics*, Vol. 226, 2007, pp. 621–644.
- <sup>53</sup>Abramov, R. V., “The Multidimensional Moment-Constrained Maximum Entropy Problem: A BFGS Algorithm with Constraint Scaling,” *Journal of Computational Physics*, Vol. 228, 2009, pp. 96–108.
- <sup>54</sup>Levermore, C., “Relating Eddington Factors to Flux Limiters,” *Journal of Quantitative Spectroscopy and Radiative Transfer*, Vol. 31, No. 2, 1984, pp. 149–160.
- <sup>55</sup>Kershaw, D., “Flux Limiting Nature’s Own Way,” Technical report, Lawrence Livermore Laboratory, 1976.
- <sup>56</sup>Cernohorsky, J. and Bludman, S. A., “Maximum Entropy Distribution and Closure for Bose-Einstein and Fermi-Dirac Radiation Transport,” *The Astrophysical Journal*, Vol. 433, No. 2, 1994, pp. 250.
- <sup>57</sup>Blyth, M. G. and Pozrikidis, C., “A Lobatto interpolation grid over the triangle,” *IMA Journal of Applied Mathematics*, Vol. 71, No. 1, 2006, pp. 153–169.
- <sup>58</sup>Peña, J. M. and Sauer, T., “On the Multivariate Horner Scheme,” *SIAM Journal on Numerical Analysis*, Vol. 37, No. 4, 2000, pp. 1186–1197.
- <sup>59</sup>Czekansky, J. and Sauer, T., “The multivariate Horner scheme revisited,” *BIT Numerical Mathematics*, Vol. 55, No. 4, 2014, pp. 1043–1056.
- <sup>60</sup>Lacis, A. A. and Oinas, V., “A Description of the Correlated k Distribution Method for Modeling Nongray Gaseous Absorption, Thermal Emission, and Multiple Scattering in Vertically Inhomogeneous Atmospheres,” *Journal of Geophysical Research*, Vol. 96, No. D5, 1991, pp. 9027–9063.
- <sup>61</sup>Soufiani, A. and Taine, J., “High temperature gas radiative property parameters of statistical narrow-band model for H<sub>2</sub>O, CO<sub>2</sub> and CO, and correlated-K model for H<sub>2</sub>O and CO<sub>2</sub>,” *International Journal of Heat and Mass Transfer*, Vol. 40, No. 4, 1997, pp. 987–991.
- <sup>62</sup>Goutiere, V., Charette, A., and Kiss, L., “Comparative Performance of Nongray Gas Modeling Techniques,” *Numerical Heat Transfer, Part B: Fundamentals*, Vol. 41, No. 3-4, 2002, pp. 361–381.
- <sup>63</sup>Lax, P. D., *Hyperbolic Systems of Conservation Laws and the Mathematical Theory of Shock Waves*, Vol. 11 of *CMBS-NSF Regional Conference Series in Applied Mathematics*, SIAM, Philadelphia, 1973.
- <sup>64</sup>Levermore, C. D., “Moment Closure Hierarchies for Kinetic Theories,” *Journal of Statistical Physics*, Vol. 83, 1996, pp. 1021–1065.
- <sup>65</sup>Godunov, S. K., “Finite-Difference Method for Numerical Computations of Discontinuous Solutions of the Equations of Fluid Dynamics,” *Matematicheskii Sbornik*, Vol. 47, 1959, pp. 271–306.
- <sup>66</sup>Harten, A., “High Resolution Schemes for Hyperbolic Conservation Laws,” *Journal of Computational Physics*, Vol. 49, 1983, pp. 357–393.
- <sup>67</sup>Einfeldt, B., “On Godunov-Type Methods for Gas Dynamics,” *SIAM Journal on Numerical Analysis*, Vol. 25, 1988, pp. 294–318.
- <sup>68</sup>Barth, T. J., “Recent Developments in High Order K-Exact Reconstruction on Unstructured Meshes,” Paper 93-0668, AIAA, January 1993.
- <sup>69</sup>Venkatakrisnan, V., “On the Accuracy of Limiters and Convergence to Steady State Solutions,” Paper 93-0880, AIAA, January 1993.
- <sup>70</sup>Zhang, Z. J. and Groth, C. P. T., “Parallel High-Order Anisotropic Block-Based Adaptive Mesh Refinement Finite-Volume Scheme,” Paper 2011-3695, AIAA, June 2011.
- <sup>71</sup>Williamschen, M. J. and Groth, C. P. T., “Parallel Anisotropic Block-Based Adaptive Mesh Refinement Algorithm For Three-Dimensional Flows,” Paper 2013-2442, AIAA, June 2013.
- <sup>72</sup>Hryniewicki, M. K., Groth, C. P. T., and Gottlieb, J. J., “Parallel Implicit Anisotropic Block-Based Adaptive Mesh Refinement Finite-Volume Scheme for the Study of Fully Resolved Oblique Shock Wave Reflections,” *Shock Waves*, Vol. 25, No. 4, 2015, pp. 371–386.
- <sup>73</sup>Freret, L. and Groth, C. P. T., “Anisotropic Non-Uniform Block-Based Adaptive Mesh Refinement for Three-Dimensional Inviscid and Viscous Flows,” Paper 2015-2613, AIAA, June 2015.
- <sup>74</sup>Freret, L., Ivan, L., De Sterck, H., and Groth, C. P. T., “High-Order Finite-Volume Method with Block-Based AMR for Magnetohydrodynamics Flows,” *Journal of Scientific Computing*, Vol. 79, No. 1, 2019, pp. 176–208.
- <sup>75</sup>Freret, L., Williamschen, M., and Groth, C. P. T., “Parallel Anisotropic Non-Uniform Block-Based Adaptive Mesh Refinement for Three-Dimensional Inviscid and Viscous Flows,” submitted to the *Journal of Computational Physics*, July 2020.
- <sup>76</sup>Gao, X. and Groth, C. P. T., “A Parallel Solution-Adaptive Method for Three-Dimensional Turbulent Non-Premixed Combusting Flows,” *Journal of Computational Physics*, Vol. 229, No. 5, 2010, pp. 3250–3275.
- <sup>77</sup>Groth, C. P. T. and Northrup, S. A., “Parallel Implicit Adaptive Mesh Refinement Scheme for Body-Fitted Multi-Block Mesh,” Paper 2005-5333, AIAA, June 2005.
- <sup>78</sup>Charest, M. R. J., Groth, C. P. T., and Gülder, Ö. L., “A Computational Framework for Predicting Laminar Reactive Flows with Soot Formation,” *Combustion Theory and Modelling*, Vol. 14, No. 6, 2010, pp. 793–825.
- <sup>79</sup>Saad, Y. and Schultz, M. H., “GMRES: A Generalized Minimal Residual Algorithm for Solving Nonsymmetric Linear Equations,” *SIAM Journal for Scientific and Statistical Computing*, Vol. 7, No. 3, 1986, pp. 856–869.
- <sup>80</sup>Saad, Y., “Krylov Subspace Methods on Supercomputers,” *SIAM Journal for Scientific and Statistical Computing*, Vol. 10, No. 6, 1989, pp. 1200–1232.
- <sup>81</sup>Brown, P. N. and Saad, Y., “Hybrid Krylov Methods for Nonlinear Systems of Equations,” *SIAM Journal for Scientific and Statistical Computing*, Vol. 11, No. 3, 1990, pp. 450–481.
- <sup>82</sup>Saad, Y., *Iterative Methods for Sparse Linear Systems*, PWS Publishing Company, Boston, 1996.
- <sup>83</sup>Mulder, W. A. and van Leer, B., “Experiments with Implicit Upwind Methods for the Euler Equations,” *Journal of Computational Physics*, Vol. 59, 1985, pp. 232–246.

<sup>84</sup>Liu, F., Swithenbank, J., and Garbett, E. S., “The Boundary Condition of the  $P_N$  Approximation Used to Solve the Radiative Transfer Equation,” *International Journal of Heat and Mass Transfer*, Vol. 35, No. 8, 1992, pp. 2043–2052.

<sup>85</sup>Roe, P. L., “Approximate Riemann Solvers, Parameter Vectors, and Difference Schemes,” *Journal of Computational Physics*, Vol. 43, 1981, pp. 357–372.

<sup>86</sup>Rosatti, G. and Begnudelli, L., “A closure-independent Generalized Roe solver for free-surface, two-phase flows over mobile bed,” *Journal of Computational Physics*, Vol. 255, 2013, pp. 362–383.